

# **Materials Informatics Approach to Material Extrusion Additive Manufacturing**

by

Daniel Braconnier

A Thesis

Submitted to the Faculty

of the

WORCESTER POLYTECHNIC INSTITUTE

in partial fulfillment of the requirements for the

Degree of Master of Science

in

Materials Science and Engineering

April 2018

APPROVED:

Prof. Amy Peterson, Major Advisor

Dr. Robert Jensen, Advisor

Prof. Richard Sisson, Head of Department

## **Abstract**

Process-structure-property relationships in material extrusion additive manufacturing (MEAM) are complex, non-linear, and poorly understood. Without proper characterization of the effects of each processing parameter, products produced through fused filament fabrication (FFF) and other MEAM processes may not successfully reach the material properties required of the usage environment. The two aims of this thesis were to first use an informatics approach to design a workflow that would ensure the collection of high pedigree data from each stage of the printing process; second, to apply the workflow, in conjunction with a design of experiments (DOE), to investigate FFF processing parameters. Environmental, material, and print conditions that may impact performance were monitored to ensure that relevant data was collected in a consistent manner. Acrylonitrile butadiene styrene (ABS) filament was used to print ASTM D638 Type V tensile bars. MakerBot Replicator 2X, Ultimaker 3, and Zortrax M200 were used to fabricate the tensile bars. Data was analyzed using multivariate statistical techniques, including principal component analysis (PCA). The magnitude of effect of layer thickness, extrusion temperature, print speed, and print bed temperature on the tensile properties of the final print were determined. Other characterization techniques used in this thesis included: differential scanning calorimetry (DSC), dynamic mechanical analysis (DMA), and scanning electron microscopy (SEM). The results demonstrated that printer selection is incredibly important and changes the effects of print parameters; moreover, further investigation is needed to determine the sources of these differences.

## **Acknowledgments**

I would first like to thank my advisor, Prof. Amy Peterson (CHE), for being such an excellent mentor throughout the entire process of this thesis. Further I would like to thank Dr. Robert Jensen (Army Research Labs) for his help with the multivariate statistical analysis. I would also like to acknowledge Anthony D'Amico (CHE), Xuejian Lyu (MTE), and Russel Lang (CE) for their help with various lab equipment.

## Table of Contents

Abstract.....	1
Acknowledgments.....	2
Table of Contents .....	3
List of Figures .....	5
List of Tables .....	8
Chapter 1: Introduction & Aims .....	9
Chapter 2: Background .....	11
2.1 Importance of Material Extrusion Additive Manufacturing .....	11
2.2 Effect of Parameters in FFF .....	11
2.3 Data Driven Experimentation .....	15
2.3 Challenges in Advancement of FFF .....	16
Chapter 3: Methodology .....	17
3.1 Materials .....	17
3.2 Differential Scanning Calorimetry (DSC) .....	17
3.3 Dynamic Mechanical Analysis (DMA) .....	18
3.4 Printing & Storage .....	18
3.5 Zortrax Print Speed Calibration .....	20
3.6 Design of Experiments.....	22
3.7 Observations .....	23
3.8 Mechanical Testing.....	23
3.9 Data Storage & Analysis.....	25
3.10 Imaging & Microscopy .....	26
Chapter 4: Results & Discussion .....	27
4.1 Printer Observations.....	27

4.2 Tensile Testing.....	31
4.2.1 Tensile Strength .....	31
4.2.2 Elongation at Break.....	32
4.2.3 Elastic Modulus .....	33
4.3 Thermal Analysis .....	34
4.3.1 DSC.....	34
4.3.2 DMA .....	35
4.4 Fractography .....	37
4.4.1 MakerBot .....	37
4.4.2 Ultimaker .....	39
4.4.3 Zortrax.....	40
4.5 Principal Component Analysis .....	42
Summary & Conclusions .....	47
Looking Forward .....	48
References.....	49
Appendix A.....	51
A.1 Print Set Form Example.....	51
A.2 Mechanical Test Form Example .....	52
Appendix B .....	54
B.1 Micrographs of 12121 & 21211 Print Conditions.....	54
B.2 Micrographs of 12222 & 21112 Print Conditions.....	56
B.3 Micrographs of 12113 & 21123 Print Conditions.....	57

## List of Figures

Figure 1: Effect of various print parameters on bond strength between printed layers [4]. ...	12
Figure 2: (Left) Effect of extrusion temperature on tensile strength, (Right) Effect of print speed on tensile strength at a 230°C extrusion temperature [5].....	13
Figure 3: (Left) Effect of layer thickness on tensile strength, (Right) Effect of print speed on tensile strength [7].....	14
Figure 4: (a) Adhesion forces of PLA as a function of print bed temperature, (b) Adhesion forces of ABS as a function of print bed temperature [9].....	14
Figure 5: Diagram representing the promise of materials informatics through the fusion of data mining tools [10]. .....	15
Figure 6: Informatics workflow approach followed through this thesis.....	16
Figure 7: Successful Zortrax M200 print, showing the orientation of the 6 tensile bars.....	18
Figure 8: (Left) Zortrax M200 [14], (Center) Ultimaker 3 [15], (Right) MakerBot Replicator 2X [16] (Images not to scale).....	19
Figure 9: (Left) M2121B sample bagged separately, (Right) 21211 print condition samples bagged together (Images after mechanical testing). .....	20
Figure 10: Z-Suite software interface, showing slider bar for setting print speed.....	21
Figure 11: Zortrax speed test +50% – sample 1. ....	21
Figure 12: (Left) A tensile bar fitting securely in the placement spacer, (Right) The tensile bar properly clamped into the Instron with the placement spacer. ....	24
Figure 13: A tensile bar from the 22213 print condition that had broken successfully within the gage length. ....	24
Figure 14: Divot that occurred due to overheating the filament feeder of the MakerBot. ....	27
Figure 15: The left nozzle of the MakerBot hitting the leftmost tensile samples, prior to rotating all MakerBot prints 90 degrees on the y-axis.....	28
Figure 16: From left to right, samples F - A; F and E suffering the most from improper deposition.....	28
Figure 17: (Left) Ultimaker printing gage length hollow. (Right) Close-up of U2222C print. ....	29

Figure 18: Zortrax 11123 print condition showing severe spider-webbing between tensile samples.....	29
Figure 19: The Zortrax fan placement and arrows showing direction of air flow.....	30
Figure 20: Average tensile strengths separated by printer type.....	31
Figure 21: Average elongations at break separated by printer type.....	32
Figure 22: Average elastic moduli separated by printer type. ....	33
Figure 23: DSC showing varying $T_g$ of the different filaments during the second heating cycle. ....	34
Figure 24: Dynamic mechanical analysis results showing the drastic difference between the tested filaments. ....	35
Figure 25: The Ultimaker white ABS filament experiencing a two stage glass transition.....	36
Figure 26: The red circle indicates where SEM samples were taken when taken from vertical bars when taken off of the print bed. The line on the bottom represents the print bed. ....	37
Figure 27: Micrograph of the M1212B sample, showing good infill quality.....	38
Figure 28: (Left) Micrograph of the M2121D sample, showing good infill quality, (Right) Micrograph of the perimeter-infill interface of the M2121D sample, showing ductile failure mechanisms.....	38
Figure 29: Micrograph of the U1222D showing poor inter-layer welding.....	39
Figure 30: (Left) Micrograph of the U2111E, showing rectangular perimeter, (Right) Micrograph of the perimeter-infill interface of the U2111E sample, showing non-homogeneous flow at layers.....	40
Figure 31: Micrograph of the Z1211B sample, showing poor infill.....	41
Figure 32: Micrograph of the Z2112B sample, showing better infill.....	41
Figure 33: (Top left) Magnitude of effect of PCs on eigenvalues of MakerBot values, (Top right) Magnitude of effect of PCs on eigenvalues of Ultimaker values, (Bottom center) Magnitude of effect of PCs on eigenvalues of Zortrax values.....	42
Figure 34: Eigenvalues from the MakerBot prints in relation to PC1 and PC2. ....	43
Figure 35: Eigenvalues from the Ultimaker prints in relation to PC1 and PC2. ....	44
Figure 36: Eigenvalues from the Zortrax prints in relation to PC1 and PC2.....	45
Figure 37: Print set form filled out for the 22121 print condition. ....	51
Figure 38: Mechanical test form filled out for the 22121 print condition (Page 1).....	52

Figure 39: Mechanical test form filled out for the 22121 print condition (Page 2)..... 53

Figure 40: (Top left) Full cross-section of M1212B sample, (Top right) Perimeter edge of M1212B sample, (Bottom center) Center of M1212B sample. .... 54

Figure 41: (Top left) Full cross-section of M1212D sample, (Top right) Perimeter edge of M1212D sample, (Bottom center) Center of M1212D sample..... 55

Figure 42: (Top left) Full cross-section of U1222D sample, (Top right) Perimeter edge of U1222D sample, (Bottom center) Center of U1222D sample..... 56

Figure 43: (Top left) Full cross-section of U2111E sample, (Top right) Perimeter edge of U2111E sample, (Bottom center) Center of U2111E sample..... 56

Figure 44: (Top left) Full cross-section of Z1211B sample, (Top right) Perimeter edge of Z1211B sample, (Bottom center) Center of Z1211B sample. .... 57

Figure 45: (Top left) Full cross-section of Z2112B sample, (Top right) Perimeter edge of Z2112B sample, (Bottom center) Center of Z2112B sample. .... 58



## List of Tables

Table 1: Print parameter set for each print condition and the corresponding print condition ID. ....	22
Table 2: Positive and negative correlations seen from PCA for MakerBot prints.....	44
Table 3: Positive and negative correlations seen from PCA for Ultimaker prints.....	45
Table 4: Positive and negative correlations seen from PCA for Zortrax prints.....	46

## Chapter 1: Introduction & Aims

Material extrusion additive manufacturing (MEAM) is a form of rapid prototyping that offers the potential for reduction of cost and time as well as the possibility to create complex structures that are difficult or impossible to machine with common manufacturing techniques. These advantages have led to the use of MEAM in a variety of industries such as aerospace, architecture, and medical devices [1].

Fused filament fabrication (FFF) is a MEAM technique that has become widely accessible to the consumer market. FFF allows consumers to produce replacement parts and entire products while only having to pay for the material used in the printing process [2]. Mobile and distributed manufacturing can be transformative for in-field applications, wherein replacement parts and products can be created for instant usage rather than waiting the lead time normally associated with common manufacturing.

It is important to note that MEAM processes like FFF rely on a multitude of processing parameters. Without proper characterization of the effects of each processing parameter, parts produced through FFF and other MEAM processes may fail to reach the properties required of the usage environment. Understanding the magnitude of effect each print parameter has on the final product will increase the success and properties of each print. Extrusion temperature, layer thickness, print bed temperature, and print speed are print parameters suspected of having the most effect on final print properties. While these parameters have been previously investigated, their interactions are nonlinear, complicating analysis and resulting in conflicting reports in the literature.

The two aims of this thesis were to 1) Use an informatics approach to design a workflow that would ensure the collection of high pedigree data from each stage of the printing process; 2) Apply the workflow, in conjunction with a design of experiments (DOE), to investigate FFF processing parameters.

MakerBot Replicator 2X, Ultimaker 3, and Zortrax M200 printers were used to fabricate ASTM D638 Type V tensile bars from acrylonitrile butadiene styrene (ABS) filament. Data was analyzed using multivariate statistical techniques, including principal component analysis (PCA). The magnitude of effect of layer thickness, extrusion temperature, print speed, and print bed temperature on the tensile properties of the final print were determined. Other characterization

techniques used in this thesis included: differential scanning calorimetry (DSC), dynamic mechanical analysis (DMA), and scanning electron microscopy (SEM). The results of this study will greatly advance our fundamental understanding of the MEAM process and advance process qualification for MEAM, which will improve reliability, safety, and economics while reducing material and energy waste.

## **Chapter 2: Background**

### *2.1 Importance of Material Extrusion Additive Manufacturing*

Material extrusion additive manufacturing (MEAM) is a form of rapid prototyping that offers the potential for reduction of cost and time as well as the possibility to create complex structures that are difficult or impossible to machine with common manufacturing techniques. These advantages have led to the use of MEAM in a variety of industries such as aerospace, architecture, and medical devices [1].

Fused filament fabrication (FFF) is a MEAM technique that has become widely accessible to the consumer market. FFF allows consumers to produce replacement parts and entire products while only having to pay for the material used in the printing process [2].

The advent of a new consumer-centric era demonstrates that manufacturing can be done on-site and with minimal training. Mobile and distributed manufacturing can be transformative for in-field applications, wherein replacement parts and products can be created for instant usage rather than waiting the lead time normally associated with common manufacturing. In-field MEAM can greatly decrease the logistical burdens associated with repair and shipment of goods to deployed military personnel [3]. However, it is important to note that MEAM processes like FFF rely on a multitude of processing parameters. Without proper characterization of the effects of each processing parameter, parts produced through FFF and other MEAM processes may fail to reach the properties required of the usage environment.

### *2.2 Effect of Parameters in FFF*

Lack of product consistency is a major issue associated with the FFF process. Understanding the magnitude of effect each print parameter has on the final product will increase the success and properties of each print. Extrusion temperature, layer thickness, print bed temperature, and print speed are print parameters suspected of having the most effect on final print properties.

Extrusion temperature has been shown to have a strong effect on tensile strength. Coogan and Kazmer of UMass Lowell tested the effects of print bed temperature, print speed, extrusion

temperature, layer width, and layer thickness on the bond strength of the prints. The two found that printing at the highest temperature a print material can handle before degrading will maximize the bond strength of each print layer. It is worth noting that Coogan and Kazmer did not see a drastic effect of print speed or print bed temperature on the mechanical properties of the prints. The effect of print speed may decrease as the extrusion temperature is increased [4]. A decrease in effect of print speed at higher extrusion temperatures was also seen by Davis et al. of the National Institute of Standards and Technology. Davis found that the tear energy of the prints increased by up to 500% when printed at an extrusion temperature of 250°C compared to the prints printed with an extrusion temperature of 210°C. The prints printed at 230°C with a print speed of 100mm/s only increased in tear energy by about 5% compared to the prints printed at 230°C with a print speed of 1mm/s [5].

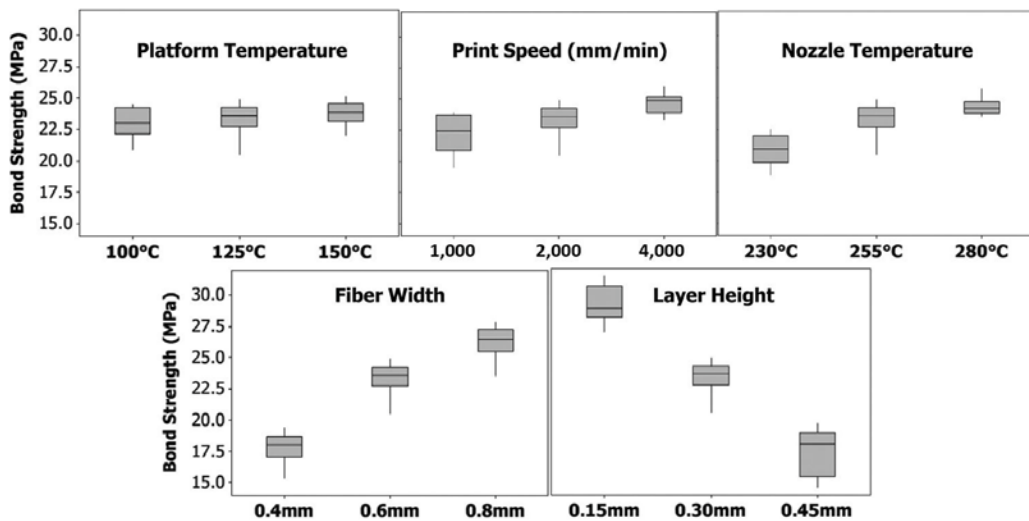


Figure 1: Effect of various print parameters on bond strength between printed layers [4].

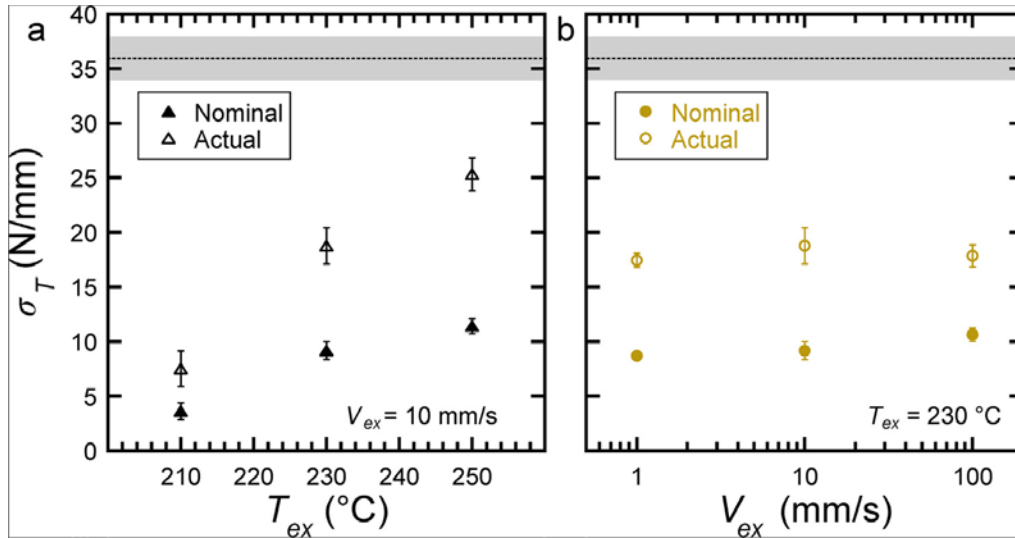


Figure 2: (Left) Effect of extrusion temperature on tensile strength, (Right) Effect of print speed on tensile strength at a 230°C extrusion temperature [5].

Tensile strength has also been correlated to layer thickness and print speed. Christiyan et al. from the Ramaiah Institute of Technology investigated the effects of varying layer thickness and print speed on the tensile properties of an ABS + hydrous magnesium silicate composite. Throughout this experiment the extrusion temperature and build plate temperature were kept at 190°C and 70°C, respectively. The infill density of the printed specimens was set to 60%. The print conditions were completed with layer thicknesses of 0.2mm, 0.25mm, and 0.3mm and print speeds of 30mm/s, 40mm/s, and 50mm/s. For all print cases, it was found that an increase in print speed led to a substantial decrease in tensile strength. This decrease in strength became more drastic as the layer thickness increased. The increase in layer thickness also had an effect on the maximum tensile strength reached for each print condition [6]. Li et al. from Tianjin University further investigated the effects of layer thickness and print speed on the mechanical properties of FFF prints. The printed tensile specimens were of poly(-lactic-acid) (PLA). The PLA was printed at an extrusion temperature of 210°C with an infill density of 100%, print speed of 80mm/s, and with layer thicknesses ranging from 0.05mm to 0.35mm at steps of 0.05mm. Li et al. discovered that tensile strength decreased with increasing layer thickness (Figure 3) [7].

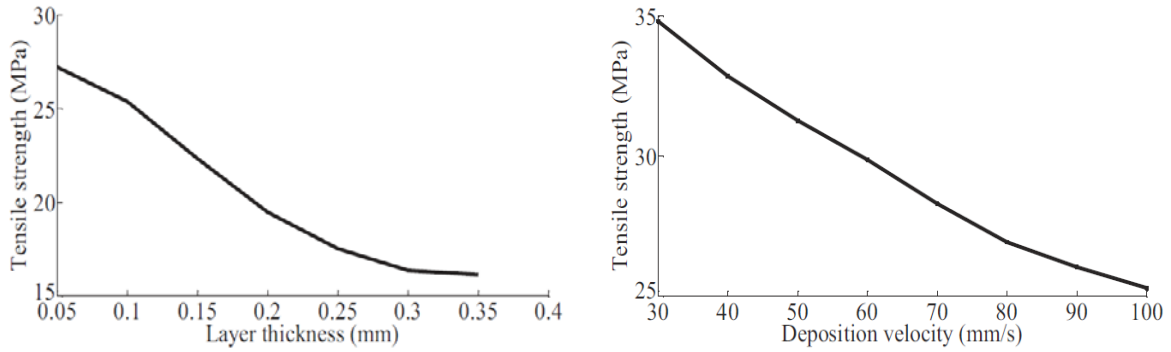


Figure 3: (Left) Effect of layer thickness on tensile strength, (Right) Effect of print speed on tensile strength [7].

Print bed temperature plays an important part in the adhesion of the first extruded layers to the build plate. However, according to literature, this parameter has little to no effect on adhesion between subsequent layers [8]. Spoerk et al. of Montanuniversitaet Leoben found that PLA and ABS have better print bed adhesion when the build plate is at a high temperature of 120°C. Both ABS and PLA samples were tested on glass and polyimide (PI) build plate surfaces. The PLA was found to have the best adhesion to both print surfaces at a temperature above the print materials glass transition temperature ( $T_g$ ). The ABS had better adhesion to the PI film surface rather than to the glass build plate; though the print bed adhesion did increase on both bed materials when the print bed temperature was above the  $T_g$  of ABS [9].

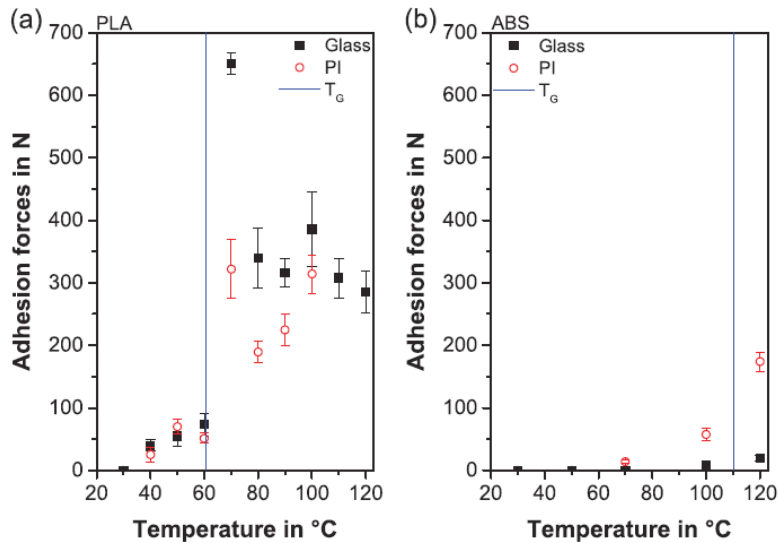


Figure 4: (a) Adhesion forces of PLA as a function of print bed temperature, (b) Adhesion forces of ABS as a function of print bed temperature [9].

### 2.3 Data Driven Experimentation

Process-structure-property relationships in MEAM are not linear and the fundamental understanding of these relationships are rarely defined by a singular narrow-focused experiment. Analyzing multivariate datasets can help better understand the non-linearity of the multi-parameter relationships associated with FFF. Materials informatics opens the frame of reference of the data collected and allows the surveying of complex multiscale information in a statistically robust and meaningful manner (Figure 5) [10]. Statistical analysis software/tools can compare the magnitudes of various process-structure-property relationships from large data pools collected through the holistic materials informatics workflow.

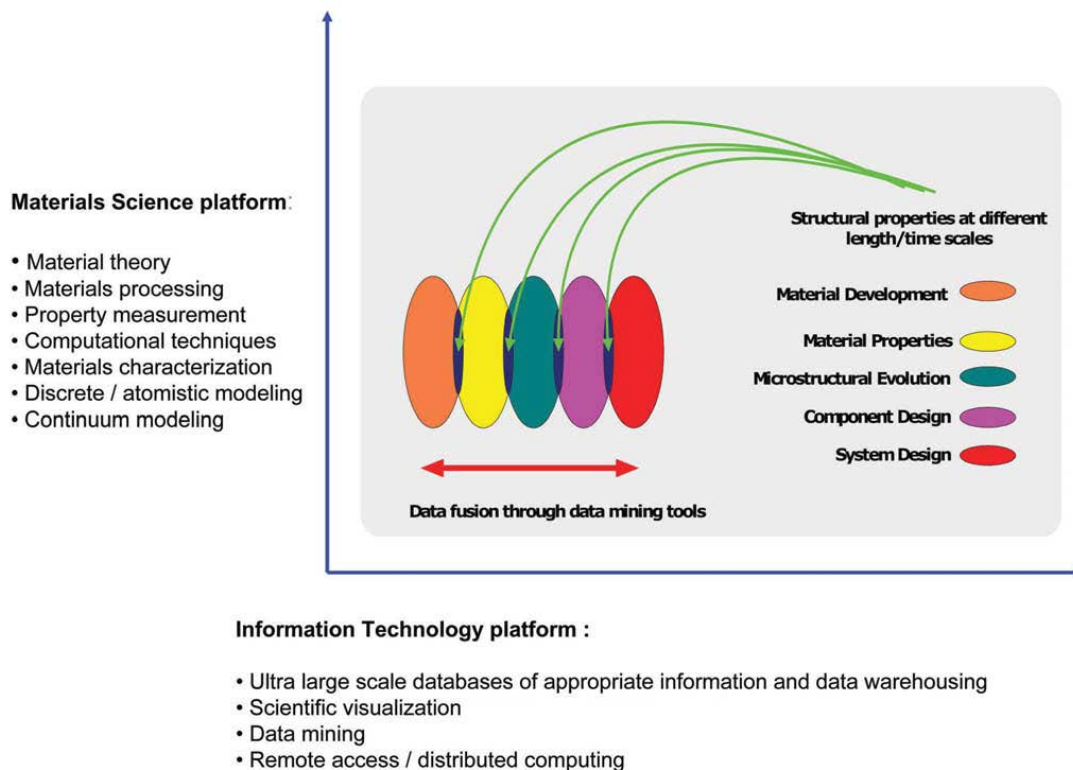


Figure 5: Diagram representing the promise of materials informatics through the fusion of data mining tools [10].



### 2.3 Challenges in Advancement of FFF

Non-linear relationships in FFF have led to conflicting discoveries on the effect of certain printing parameters. Opposing discoveries are possible due to the lack of standardization in the printing processes used. As referenced above, print speed can have a great effect or nearly none at all on the resulting properties of the print specimen [ [4]- [7]].

This thesis aims to alleviate some of the ‘guess and check’ with FFF process-structure-property relationships by accessing data collected from every stage of the printing process (Figure 6). Further, by utilizing multivariate statistical analysis, the fundamental understanding of non-linear FFF relationships can be better defined.

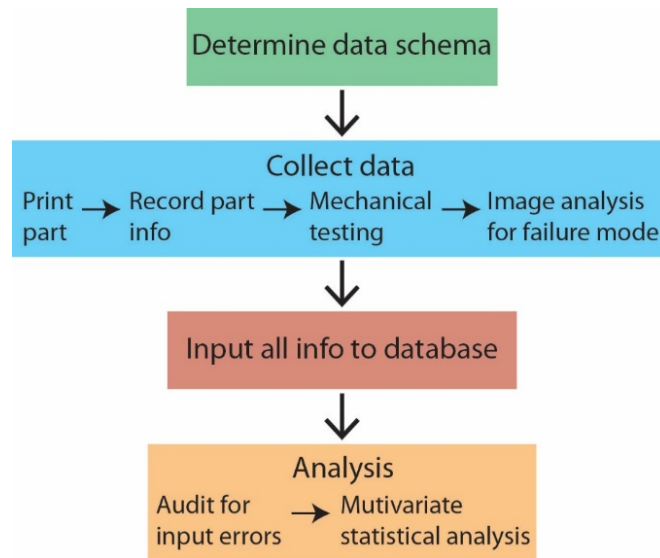


Figure 6: Informatics workflow approach followed through this thesis.

## Chapter 3: Methodology

### 3.1 Materials

Acrylonitrile butadiene styrene (ABS) filament was used to print ASTM Type V tensile bars for the D638 standard mechanical testing. ABS is a common copolymer used for fused filament fabrication (FFF) due to easy processability and good mechanical properties [11]. ABS filament was procured from two manufacturers. MakerBot Natural ABS filament (Lot ID: 003991) was used for the MakerBot Replicator 2X and Zortrax M200 printers. This filament has an average diameter of 1.75mm and is advertised to have few additives. The Ultimaker 3 cannot use 1.75mm diameter filament, so Ultimaker White ABS filament (Lot ID: 1622) with a diameter of 2.85mm was used for the Ultimaker 3 prints.

### 3.2 Differential Scanning Calorimetry (DSC)

A Netzsch DSC Polyma 214 was used to characterize the thermal properties of each ABS filament. DSC can be used to determine the heat capacity, heat flow, glass transition temperature, crystallization temperature, and melting temperature of a given sample [12].

An empty reference pan and a sample pan are prepared and placed in the test chamber. Each ABS filament sample weighed an average of  $13.5\text{mg} \pm 0.2\text{mg}$ . MakerBot red ABS, MakerBot natural ABS, and Ultimaker white ABS filaments were tested.

All DSC tests began after equilibration at  $30^\circ\text{C}$  for 20 minutes. Then, the samples were heated to  $255^\circ\text{C}$  at the rate of  $0.50^\circ\text{C}/\text{min}$ , equilibrated at  $255^\circ\text{C}$  for 20 minutes, and cooled at a rate of  $0.50^\circ\text{C}/\text{min}$  to  $30^\circ\text{C}$ .

### 3.3 Dynamic Mechanical Analysis (DMA)

A Netzsch Artemis DMA 242 E was used to analyze the viscoelastic behavior of the ABS filament as a stress is applied [13]. Sample length for all samples was 8.9mm as determined by the separation of the grips. Tensile mode DMA was then conducted from -50°C to 120°C at a heating rate of 2 °C/min with a target amplitude of 1 µm and a frequency of 1 Hz.

### 3.4 Printing & Storage

SolidWorks 2017 was used to create the stereolithographic (STL) file that was input into each print software. The same file of six type V tensile bars (Figure 7) was used for each of the 18 print conditions (Table 1) for a total of 108 tensile bars. Bars were printed in sets of six to ensure that at least 3 successful tensile tests were performed per print condition.

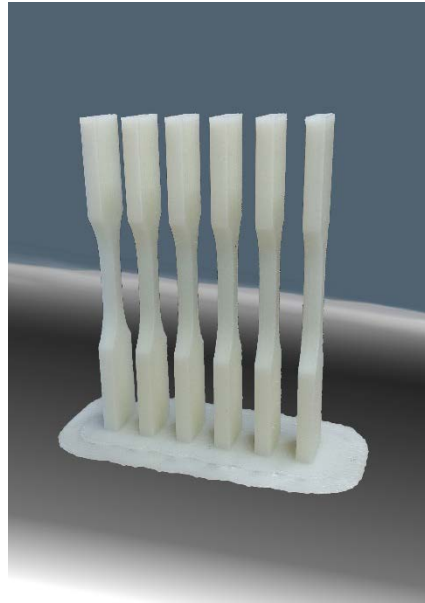


*Figure 7: Successful Zortrax M200 print, showing the orientation of the 6 tensile bars.*

The print softwares used were Simplify3D and Z-Suite. Simplify3D was used to produce the gcode for the MakerBot and Ultimaker prints. Z-Suite had to be used for the Zortrax prints because

the Zortrax M200 only functions with the proprietary zcode. Z-Suite was far more limiting in which print parameters could be changed.

The three printers used to print the tensile bars were: (1) MakerBot Replicator 2X, (2) Ultimaker 3, and (3) Zortrax M200 (Figure 8). The MakerBot and Ultimaker had two extrusion nozzles. For all prints, only the right extrusion nozzle was used on either printer. The Zortrax had only one extrusion nozzle. Each printer had a different style of print bed. The MakerBot had a slate-like material for the print bed. A polyimide (PI) film was used on top of the MakerBot print bed. A coating of ABS slurry was used on top of the PI film so the prints would have better print bed adhesion. The Ultimaker had a glass print bed. For good print bed adhesion, the glass bed was coated with a glue stick. The Zortrax had a metal perforated print bed and did not require any additional materials for good print bed adhesion.



Figure 8: (Left) Zortrax M200 [14], (Center) Ultimaker 3 [15], (Right) MakerBot Replicator 2X [16] (Images not to scale).

Individual print samples were bagged and labeled, then the print sets of six were grouped and bagged by profile (Figure 9). Each sample was labeled from A to F, with A being the first tensile specimen printed in the set of six and F being the last printed. Samples sets from all profiles were stored in as similar of an environment as possible. When prints were completed, bagged sample sets were stored in the same drawer to acclimate to the lab environment for at least 2 days before

tensile testing. Further, all print conditions were moved together as one unit such that all the samples would experience the same environmental changes.

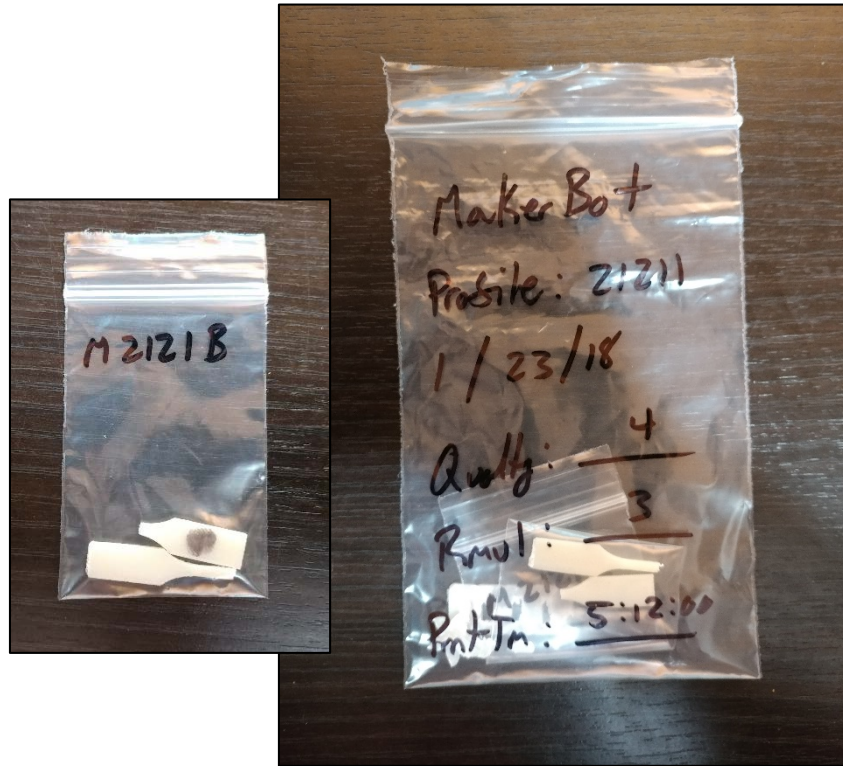


Figure 9: (Left) M2121B sample bagged separately, (Right) 21211 print condition samples bagged together (Images after mechanical testing).

### 3.5 Zortrax Print Speed Calibration

Z-Suite utilizes a slider bar instead of numerical input for setting the print speed of prints (Figure 10). To calibrate print speeds of the Zortrax M200, a series of test prints had to be performed. A STL file of a 5cm line was created (Figure 11) and printed at the 0%, -50%, and +50% speed designated by the Z-Suite software. The file was printed three times at each speed and video was taken of each print to determine the average print speed. The print average print speeds from the lowest to highest were determined to be  $10\text{mm/s} \pm 0.2\text{mm/s}$  to  $35\text{mm/s} \pm 1\text{mm/s}$ , with  $22\text{mm/s} \pm 0.5\text{mm/s}$  as the default speed. After these speeds were determined, the print parameters could be set for the print conditions.

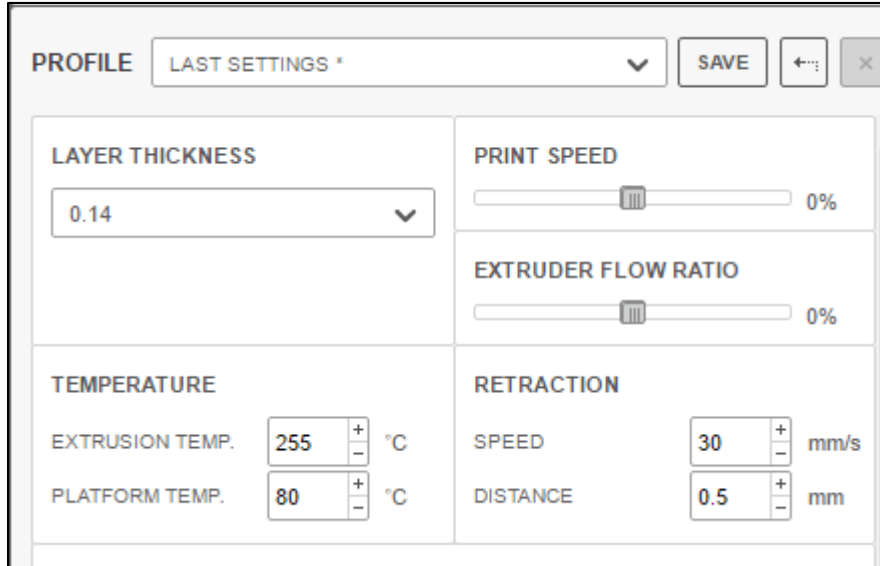


Figure 10: Z-Suite software interface, showing slider bar for setting print speed.

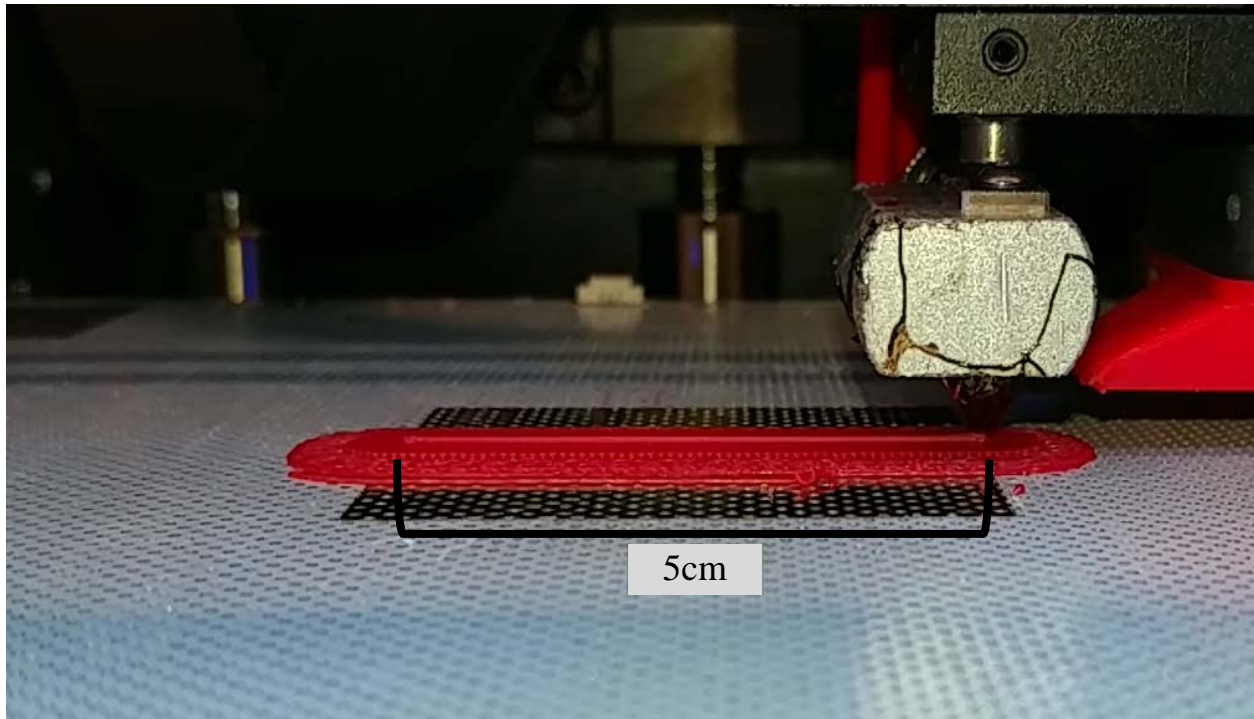


Figure 11: Zortrax speed test +50% – sample 1.

### 3.6 Design of Experiments

Print conditions were designed using the SAS JMP 14 statistical software. Extrusion temperature (ET), layer thickness (LT), print bed temperature (PBT), print speed (PS), and printer were used as the changeable variables. For all print conditions, raster orientation was set to 45°/-45°, print orientation was set to 90° from the print bed, and print infill was set to 100% (or ‘maximum’ set through Z-Suite). All other print parameters, set by the printer and print software, were left alone. Print condition IDs were standardized to ensure easy sharing of data. The print condition IDs were built of five numbers; each number corresponding to a specific parameter. Those parameters with a low or high value were set to be 1 or 2, respectively. The designations for each printer were as follows: 1 = MakerBot Replicator 2X, 2 = Ultimaker 3, and 3 = Zortrax M200 (Table 1).

Table 1: Print parameter set for each print condition and the corresponding print condition ID.

<b>Print Condition ID</b>	<b>ET (°C)</b>	<b>LT (µm)</b>	<b>PBT (°C)</b>	<b>PS (mm/sec)</b>	<b>Printer</b>
22111	255	290	80	10	MakerBot Replicator 2X
22121	255	290	80	35	MakerBot Replicator 2X
12121	210	290	80	35	MakerBot Replicator 2X
11211	210	140	100	10	MakerBot Replicator 2X
11221	210	140	100	35	MakerBot Replicator 2X
21211	255	140	100	10	MakerBot Replicator 2X
22222	255	290	100	35	Ultimaker 3
21112	255	140	80	10	Ultimaker 3
22222	255	290	100	35	Ultimaker 3
11112	210	140	80	10	Ultimaker 3
12222	210	290	100	35	Ultimaker 3
11112	210	140	80	10	Ultimaker 3
12113	210	290	80	10	Zortrax M200
12213	210	290	100	10	Zortrax M200
22213	255	290	100	10	Zortrax M200
21123	255	140	80	35	Zortrax M200
21223	255	140	100	35	Zortrax M200
11123	210	140	80	35	Zortrax M200

### *3.7 Observations*

Observations related to printing and testing were recorded. Standardized forms were used to track the printing and mechanical testing processes (Appendix A). Ambient relative humidity, temperature, and lab business were tracked on each form because it is unknown if these environmental conditions play a role in the final print properties. The humidity was measured with an analog hygrometer. Ambient temperature stayed near constant ( $\pm 1^\circ\text{C}$ ) in the laboratory space at a temperature of  $21^\circ\text{C}$ .

Prints were qualitatively assessed for print quality, ease of removal from the build plate, and general print time. The print quality and removal from build plate were determined on a scale of one to five, with one being the worst and five being the best of each criterion. Print time was determined by the estimated time to print or the print completion time; both were displayed on the printer interface. The dimensions of each sample were recorded with digital calipers and compared against the STL file dimensions. An overall dimensional accuracy was determined from the collected information.

### *3.8 Mechanical Testing*

An Instron 5567A load frame with a 10kN load cell was used to perform all mechanical tests. All tensile tests were performed in accordance with ASTM D638-14. The strain rate for all tensile tests was 0.1mm/sec. The Instron software, BlueHill 3, recorded all data from the mechanical tests.

Samples were secured in the tensile clamps with a placement spacer (Figure 12). The spacer was a negative of the tensile specimen gage length and was designed to protect the samples from premature fracture during installation and keep placement of samples consistent during testing. Some print conditions had too many print artifacts and prevented use of the placement spacer.



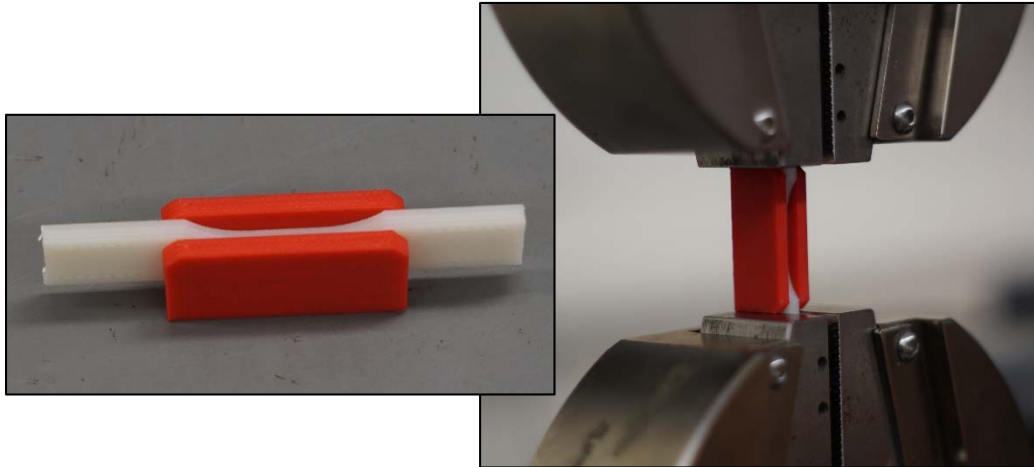


*Figure 12: (Left) A tensile bar fitting securely in the placement spacer, (Right) The tensile bar properly clamped into the Instron with the placement spacer.*

Tensile testing data collected was used to calculate tensile strength, elongation at break, and elastic modulus for each successful test. A tensile test was successful if the fracture occurred within the gage length (Figure 13) of the tensile bar.

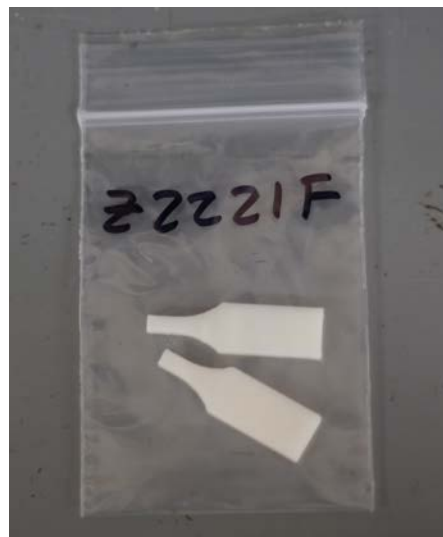


*Figure 13: A tensile bar from the 22213 print condition that had broken successfully within the gage length.*

### 3.9 Data Storage & Analysis

All raw data was collected as CSV files. The raw data was then referenced using a separate analysis worksheet using Microsoft Excel 2016. Raw data and analysis files were stored in the same parent folder then organized into subfolders. A grouped summary worksheet was utilized to call on the most relevant analysis to generate visual displays of various trends discovered. The SAS JMP 14 software was utilized to further uncover relationships that could not be so easily displayed with Microsoft Excel.

Principal component analysis (PCA) was the multivariate statistical technique used with the SAS JMP 14 software. PCA is used for visualizing the correlations in a large data matrix ( $X$ ) by reducing  $X$  to a product of a smaller loading ( $P$ ) and score ( $T$ ) matrix [ [17], [18], [19], [20], [21]]. Matrix  $P$  and  $T$  contain the data patterns used to correlate relationships between the variables and samples, respectively (Equation 1). This orthogonal linear transformation reduces the dimensionality of  $X$  to a new set of orthogonal and uncorrelated variables, which are the principal components (PC).

*Equation 1: Relationship of matrices  $P$  and  $T$  with matrix  $X$ .*

$$X = TP^T = \sum_{i=1}^q t_i p_i^T$$

The principal components represent covariance of the original variables as normalized eigenvectors. The first principal component has the highest variance vector score, followed by the second principal component, and so forth. Many complex data set variations can be reduced to 2 principal components. Principal component analysis is sensitive to the scaling magnitude of the original variables. SAS JMP 14 by default normalizes  $X$  by subtracting the mean and dividing by its standard deviation to generate a standardized data matrix suitable for PCA.

### *3.10 Imaging & Microscopy*

Close-up photographs of the best and worst print conditions from each printer were recorded with a Sony Alpha 6000 mirrorless camera. Micrographs were taken of the same fracture surfaces with a scanning electron microscopy (SEM). The SEM micrographs were analyzed to better understand fracture mechanisms experienced during mechanical testing. The entire cross-section, infill-perimeter interface, and infill of each sample were imaged. All micrographs can be found in Appendix B. Segregated by printer, the print conditions with the lowest and highest tensile strength were selected for imaging. These print conditions were observed: 12121, 21211, 12222, 21112, 12113, 21123.

## Chapter 4: Results & Discussion

### 4.1 Printer Observations

The Makerbot was located in a chemical fume hood, which reduced the potential effects of lab disturbances and environmental fluctuations. The MakerBot Replicator 2X extrusion nozzle regularly clogged when printing 100 $\mu$ m thick layers. As a result, the original DOE boundaries for layer thickness had to be changed from 100 $\mu$ m and 200 $\mu$ m to the next available Zortrax compatible thicknesses: 140 $\mu$ m and 290 $\mu$ m. Simplify3D on default sets MakerBot print codes to have a fan speed of 0%. With the extruder fan off the filament feeding section would regularly overheat. The excess heat in the gear box caused the filament to soften such that the gears would grid out a divot in the filament; ultimately stopping extrusion (Figure 14). The fan speed for all later MakerBot prints was set to 70% [22].



Figure 14: Divot that occurred due to overheating the filament feeder of the MakerBot.

Simplify3D on default sets MakerBot print codes to have retraction off. Too much retraction would cause the feeder gears to develop a divot in the filament, thus causing extrusion to cease. Through trial and error, it was determined retraction had to be set to 1.5mm to successfully print without a jam at any layer thickness. The STL file was reoriented along the y-axis to avoid the left nozzle of the MakerBot hitting the samples and disrupting the printing process (Figure 15).

MakerBot printed samples were strongly adhered to the rafts. All samples had to be removed by snapping the raft itself with plyers.



*Figure 15: The left nozzle of the MakerBot hitting the leftmost tensile samples, prior to rotating all MakerBot prints 90 degrees on the y-axis.*

The Ultimaker idled on average for 20mins before the first bead was laid by the extrusion nozzle. Simplify3D on default set Ultimaker print codes to have a fan speed of 0%. All three printers (as well as the printer in reference [22]) had the same 24v fan. Thus, the fan speed was set to 70% to match the MakerBot print code. The first three layers of all Ultimaker prints had a ‘weak’ deposition. Regularly, samples E and F would suffer from the worst deposition (Figure 16).

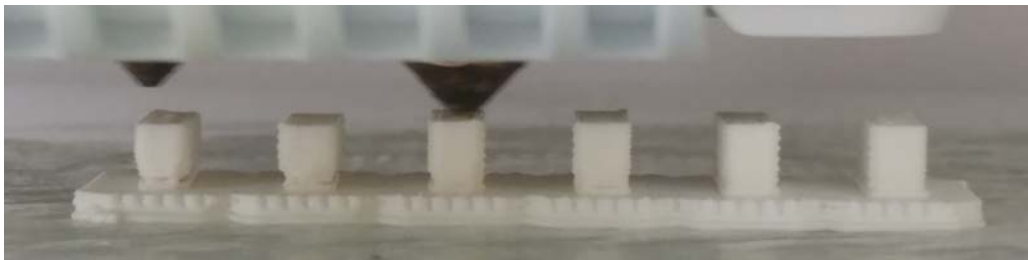


*Figure 16: From left to right, samples F - A; F and E suffering the most from improper deposition.*

The Ultimaker 3 interpreted the generated gcode as hollow in the gage length (Figure 17). Mechanical test values were drastically effected. The Ultimaker printed many unwanted features on the tensile samples, which made it difficult to use the placement spacer for mechanical testing. Print condition 12222 had the best surface finish, yet this print condition had the lowest mechanical properties.

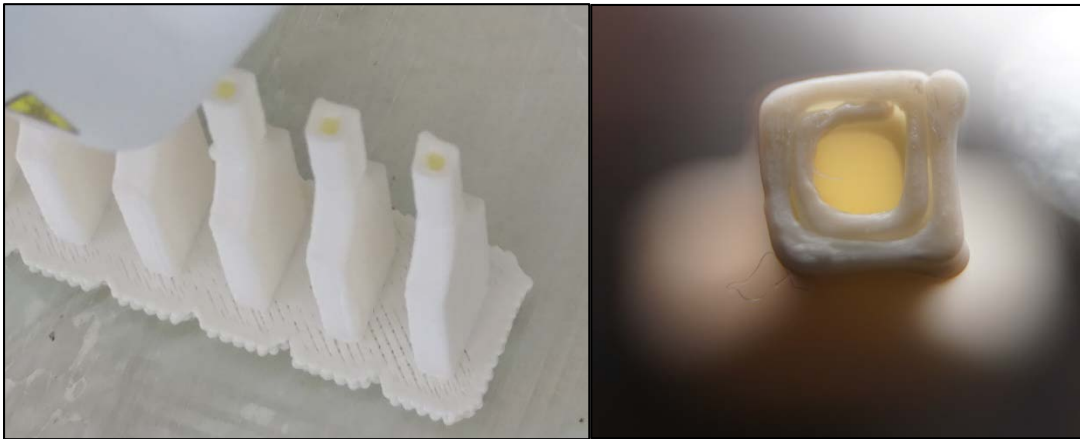


*Figure 17: (Left) Ultimaker printing gage length hollow. (Right) Close-up of U2222C print.*

Zortrax print condition 11123 had the largest amount of ‘spider-webbing’ between samples (Figure 18). ‘Spider-webbing’ increased when prints were run with lower extrusion temperatures and faster print speeds.



*Figure 18: Zortrax 11123 print condition showing severe spider-webbing between tensile samples.*

Fan placement on the Zortrax print head only cooled the area of layer deposition (Figure 19). The extruder would overheat the filament feeding section and cause the filament to soften. A 20-minute wait period with the Zortrax turned off was used to allowed the filament feeder to cool enough for another print to be started without a filament jam.

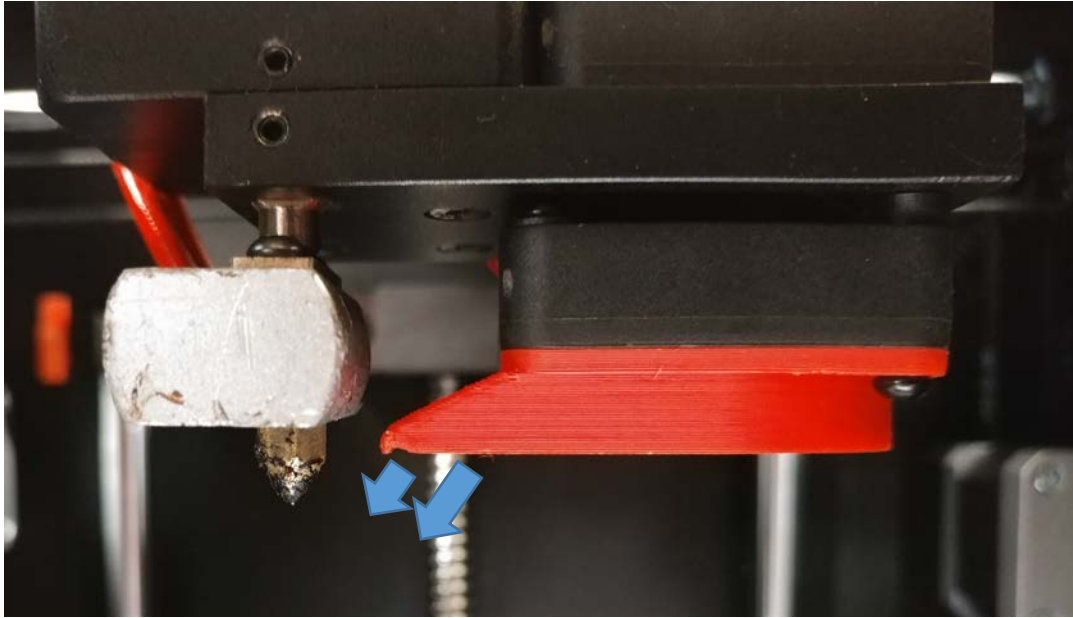


*Figure 19: The Zortrax fan placement and arrows showing direction of air flow.*

## 4.2 Tensile Testing

All the tensile strengths and elastic moduli were normalized for this section to account for the different cross-sectional areas produced by each of the three printers.

### 4.2.1 Tensile Strength

The MakerBot produced tensile bars with normalized tensile strengths above 25MPa on average. The MakerBot print conditions with extrusion temperatures set to 210°C experienced an average decrease in tensile strength of 7.37% compared to print conditions with extrusion temperatures of 255°C (Figure 20). Ultimaker print conditions with an extrusion temperature of 210°C experienced an average decrease in normalized tensile strength of 18.95% compared to print conditions with extrusion temperatures of 255°C (Figure 20). Extrusion temperature had a strong effect on the tensile strength of the Zortrax samples. Zortrax print conditions with an extrusion temperature of 210°C experienced an average decrease in normalized tensile strength of 58.72% compared to print conditions with an extrusion temperature of 255°C (Figure 20).

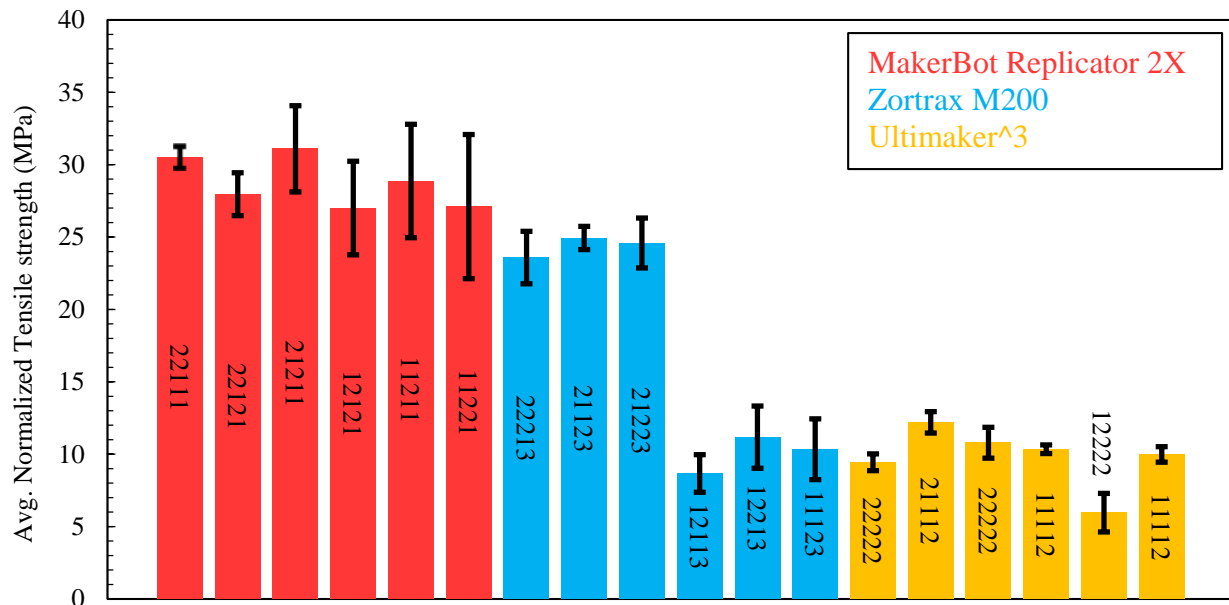


Figure 20: Average tensile strengths separated by printer type.



#### 4.2.2 Elongation at Break

Elongation at break for MakerBot print conditions decreased an average of 23.38% for print conditions with an extrusion temperature of 210°C compared to print conditions with an extrusion temperature of 255°C (Figure 21). Elongation at break for Ultimaker print conditions decreased an average 22.87% for print conditions with an extrusion temperature of 210°C compared to print conditions with an extrusion temperature of 255°C (Figure 21). Elongation at break for Zortrax print conditions decreased an average of 59.10% for print conditions with an extrusion temperature of 210°C compared to print conditions with an extrusion temperature of 255°C (Figure 21).

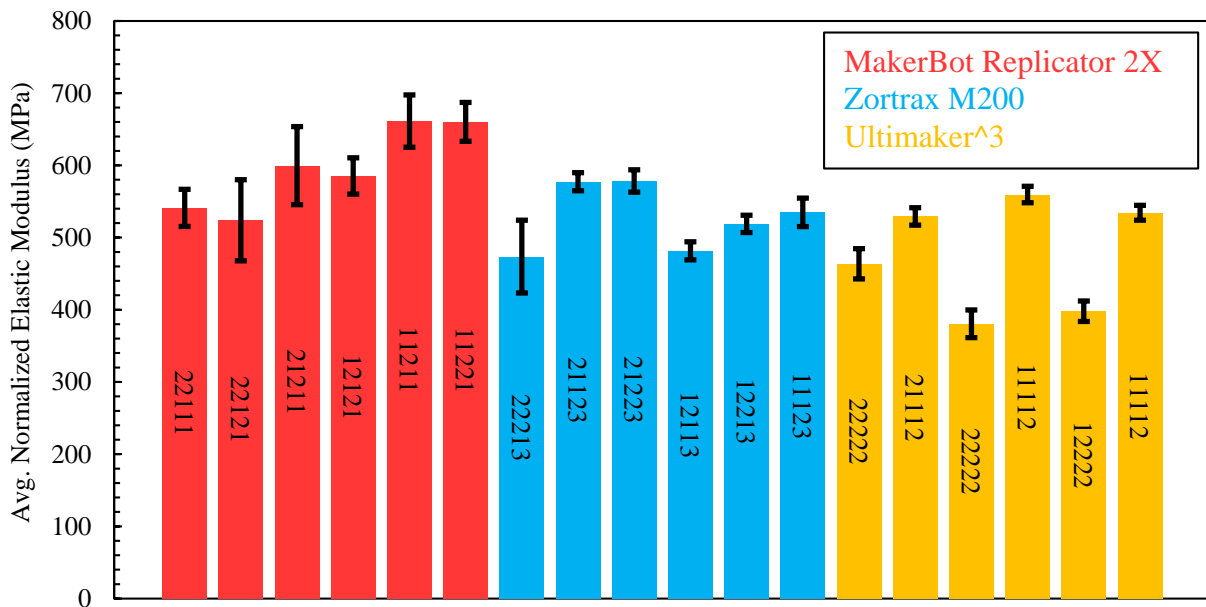


Figure 21: Average elongations at break separated by printer type.

### 4.2.3 Elastic Modulus

Extrusion temperature, print bed temperature, and print speed showed no direct effect on the elastic moduli of each print condition. MakerBot print conditions with layer thickness set to 140 $\mu\text{m}$  experienced an average increase in normalized elastic modulus of 16.42% compared to print conditions with layer thickness of 290 $\mu\text{m}$  (Figure 22). On average, Ultimaker print conditions with low end values of layer thickness (140 $\mu\text{m}$ ), print bed temperature (80 $^{\circ}\text{C}$ ), and print speed (10mm/sec) experienced an increase in normalized elastic modulus of 30.66% compared to the corresponding high end values (Figure 22). Zortrax print conditions with print speed set to 10mm/sec experienced an average decrease in normalized elastic modulus of 12.80% compared to print conditions with a print speed of 35mm/sec (Figure 22).

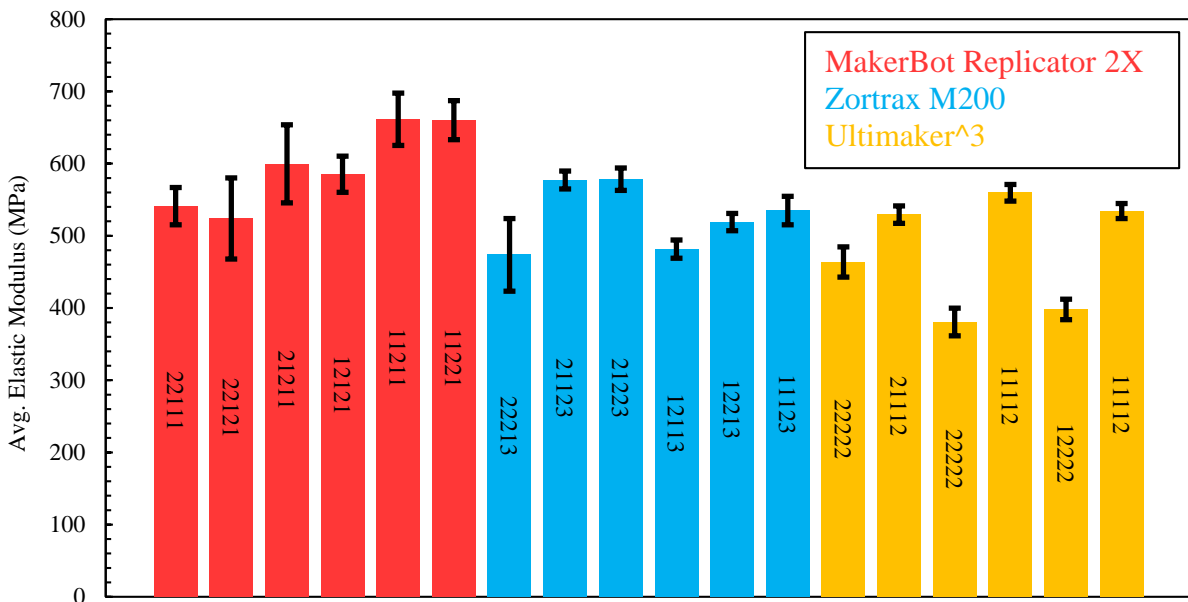


Figure 22: Average elastic moduli separated by printer type.

### 4.3 Thermal Analysis

#### 4.3.1 DSC

The MakerBot red, MakerBot natural, and Ultimaker white ABS filament glass transition temperatures ( $T_g$ ) were characterized with DSC (Figure 23). The MakerBot red filament had an average  $T_g$  of 108.25°C between the first and second heating cycle. The MakerBot natural filament had an average  $T_g$  of 108.95°C between the first and second heating cycle. The Ultimaker white filament had an average  $T_g$  of 82.1°C between the first and second heating cycle. The addition of red dye to the MakerBot red filament had effected the heat capacity of the ABS. Compared to the natural ABS filament, the red filament had a higher heat capacity. The Ultimaker white ABS had the highest heat capacity. The increase in heat capacity may be attributed to different fillers present in the material. The DSC scans for the Makerbot filaments indicated that they had the same base ABS formulation. The Ultimaker filament formulation is far different from that of the MakerBot filaments. This could be because of different relative amounts of ABS co-monomers or the addition of various plasticizers that would lower the  $T_g$ .

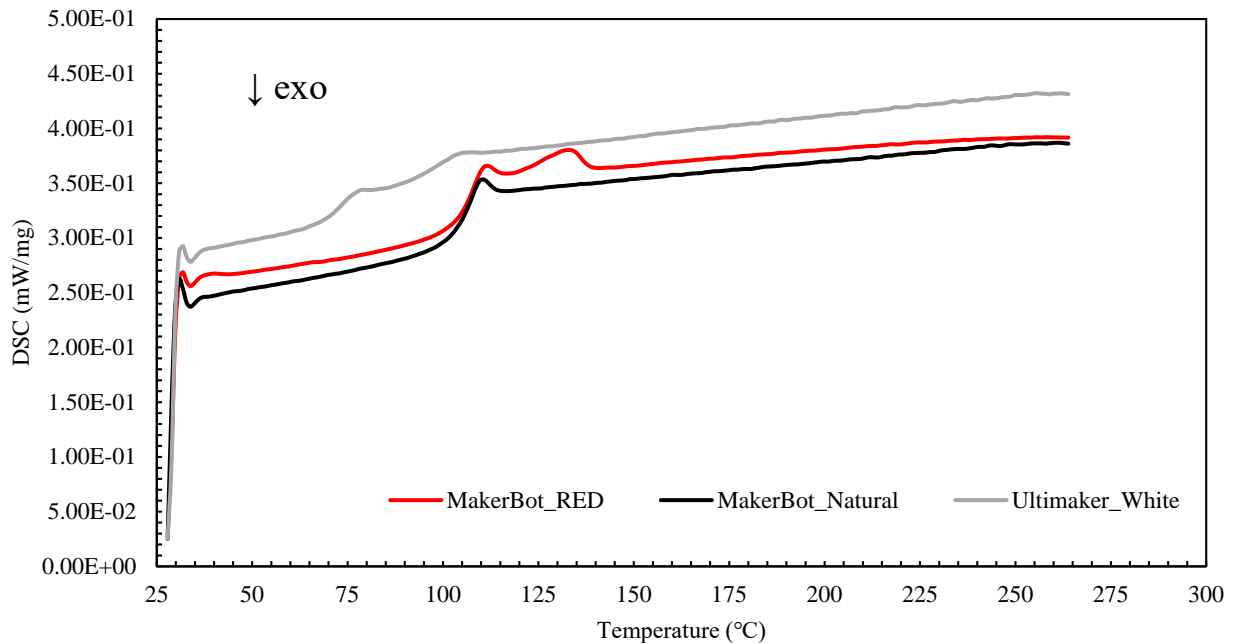


Figure 23: DSC showing varying  $T_g$  of the different filaments during the second heating cycle.

### 4.3.2 DMA

DMA was performed on the MakerBot red, MakerBot natural, and Ultimaker white ABS filament to study the viscoelastic behavior of the filament as a stress was applied. The temperature and frequency were varied and the results are summarized in Figure 24. As the temperature increased, the storage modulus ( $E'$ ) decreased. The MakerBot ABS filaments both experienced a similar glass transition around  $108^{\circ}\text{C}$ . The MakerBot natural ABS filament had  $E'$  values around 10% less than that of the MakerBot red ABS filament. This difference in stiffness could be a result of the added red pigment to the ABS filament. The Ultimaker filament had far lower  $E'$  values, meaning that the Ultimaker white ABS filament was less stiff than the Makerbot filaments.

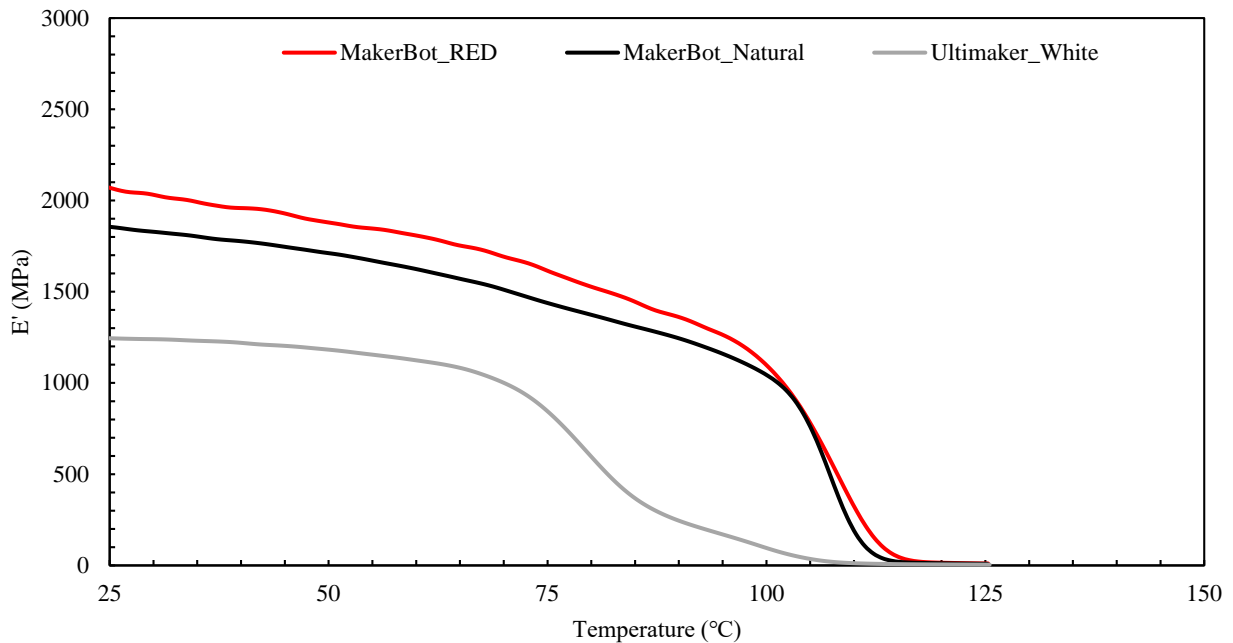


Figure 24: Dynamic mechanical analysis results showing the drastic difference between the tested filaments.

The Ultimaker filament experienced two distinct glass transitions, one around  $82^{\circ}\text{C}$  and another around  $107^{\circ}\text{C}$ . This can be seen in the DSC results (Figure 23) and more clearly in the graph of  $\tan \delta$  versus temperature (Figure 25).  $\tan \delta$  is the damping factor of the material, which expresses the fraction of mechanical energy dissipated during the cyclical loading/unloading of testing. The two glass transitions exhibited by the Ultimaker white ABS are separated by an elongated rubbery plateau [23]. This phenomenon can occur because the Ultimaker white filament may be created with different

fractions of acrylonitrile, butadiene, and styrene along with different and/or different amounts of additives than the Makerbot filaments.

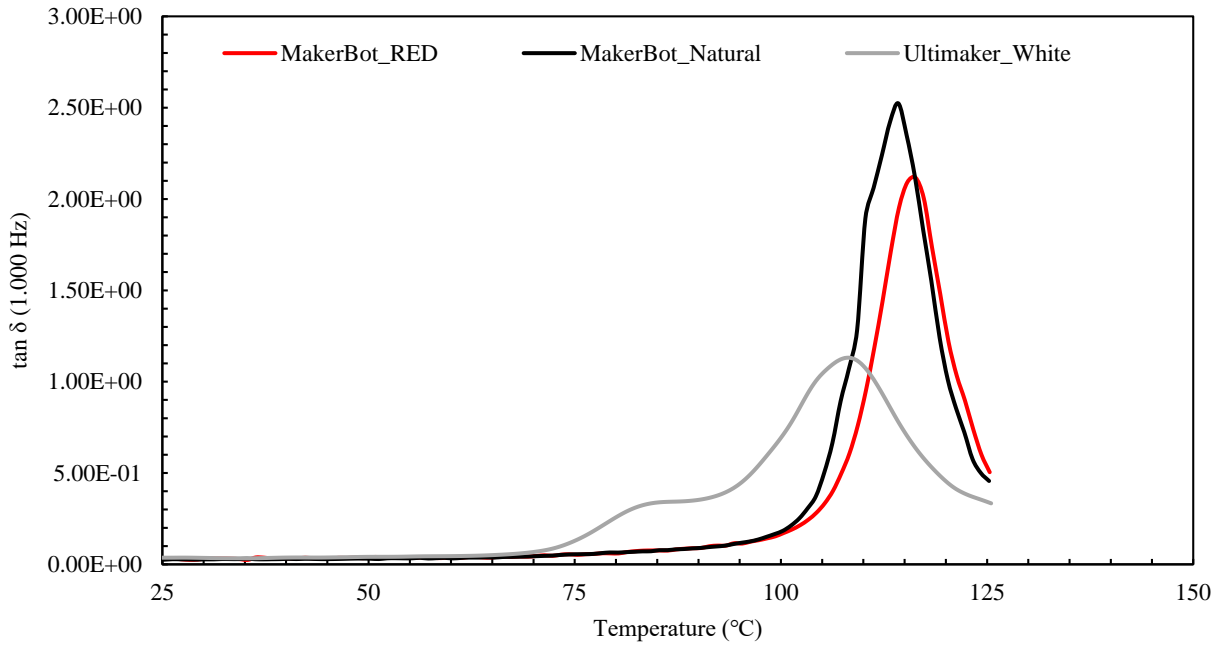


Figure 25: The Ultimaker white ABS filament experiencing a two stage glass transition.

#### 4.4 Fractography

Scanning electron microscopy (SEM) was utilized to observe material characteristics and interlayer bonding on the fracture surface of the tensile testing bars. All SEM samples that were taken from vertical bars were from the bottom portion of the printed tensile bar. A visual representation of this can be seen in Figure 26. These print conditions were observed: 12121, 21211, 12222, 21112, 12113, 21123.

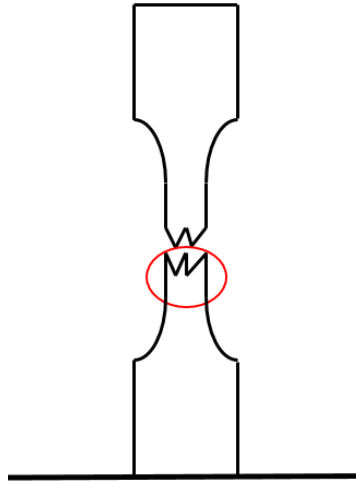
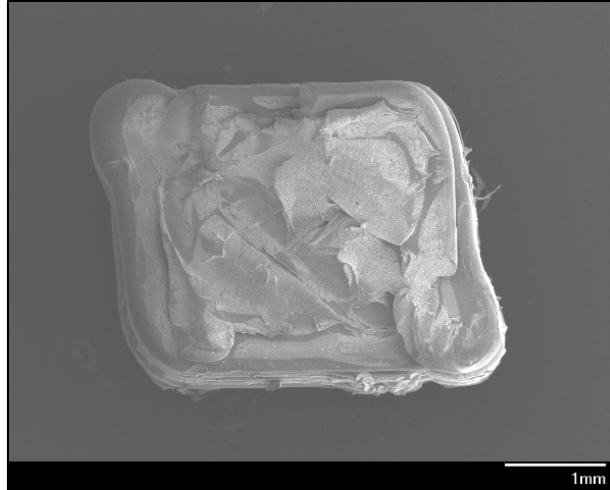


Figure 26: The red circle indicates where SEM samples were taken when taken from vertical bars when taken off of the print bed. The line on the bottom represents the print bed.

##### 4.4.1 MakerBot

The two print condition IDs observed in this section are 12121 and 21211. Figure 27 shows the full cross-section of the M1212B tensile bar. The perimeter of the print was laid in a parallelogram shape rather than a true rectangle. The parallelogram effect was due to the alternating starting points of each layer. This alternation of bead starting points were seen throughout all the MakerBot prints. Figure 27 shows that the worst of the MakerBot prints (12121) still had infill with minimal gaps between the raster pattern. The whiter areas of the cross-section show that there was some yielding during tensile testing; which was observed in the stress-strain analysis sheets.



*Figure 27: Micrograph of the M1212B sample, showing good infill quality.*

Figure 28 shows the full cross-section of the M2121D tensile bar. The perimeter was also laid in a parallelogram shape rather than a rectangular area. Figure 28 shows that the best of the MakerBot prints (21211) had infill with no gaps between the raster pattern. Furthermore, the raster pattern is indiscernible with these print conditions. The excellent inter-layer welding can be attribute to the high extrusion temperature and low print speed of the 21211 print conditions. The whiter areas of the cross-section show that there was some yielding during tensile testing; which was observed in the stress-strain analysis sheets. The pitting observed in Figure 28 demonstrates that the 21211 prints had experienced a more ductile fracture than that of the 12121 print condition.

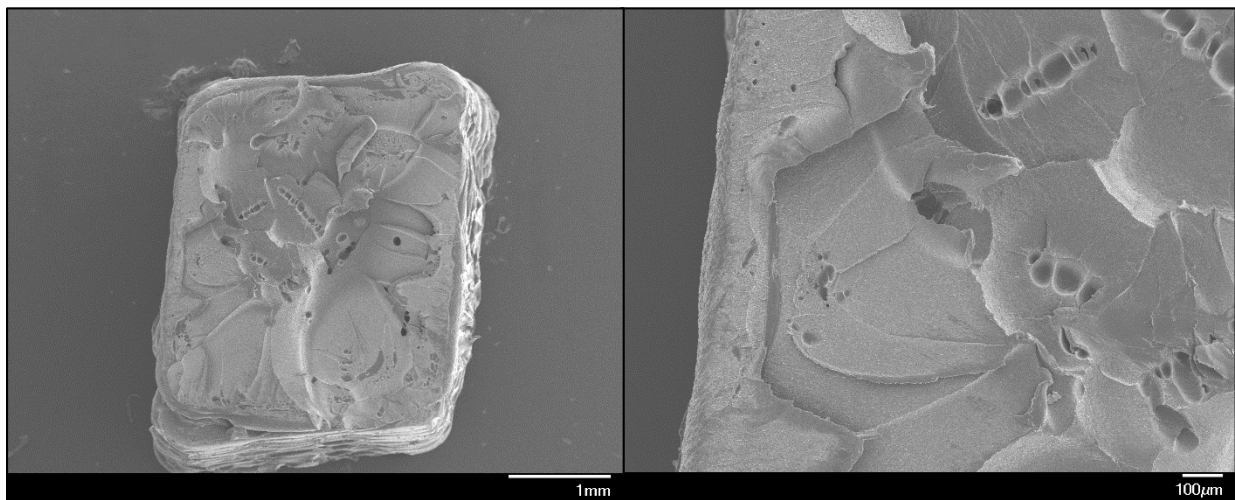


*Figure 28: (Left) Micrograph of the M2121D sample, showing good infill quality, (Right) Micrograph of the perimeter-infill interface of the M2121D sample, showing ductile fracture mechanisms.*

#### 4.4.2 Ultimaker

The two print condition IDs observed in this section are 12222 and 21112. There are no micrographs of Ultimaker infill because the Ultimaker prints interpreted the gcode as hollow in the gage length of the tensile bars. Figure 29 shows the full cross-section of the U1222D tensile bar. The perimeter of the print was laid counterclockwise from the top left of the micrograph. The perimeter start and stop points left two protrusions up through the gage length of all Ultimaker prints. Figure 29 show that the 12222 prints had minimal layer to layer welding and large gaps between the outer and inner perimeters. The whiter areas of the cross-section show where the layer to layer welding was formed.

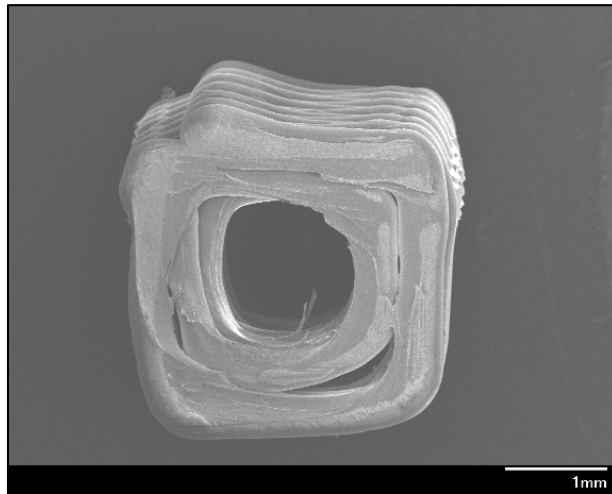
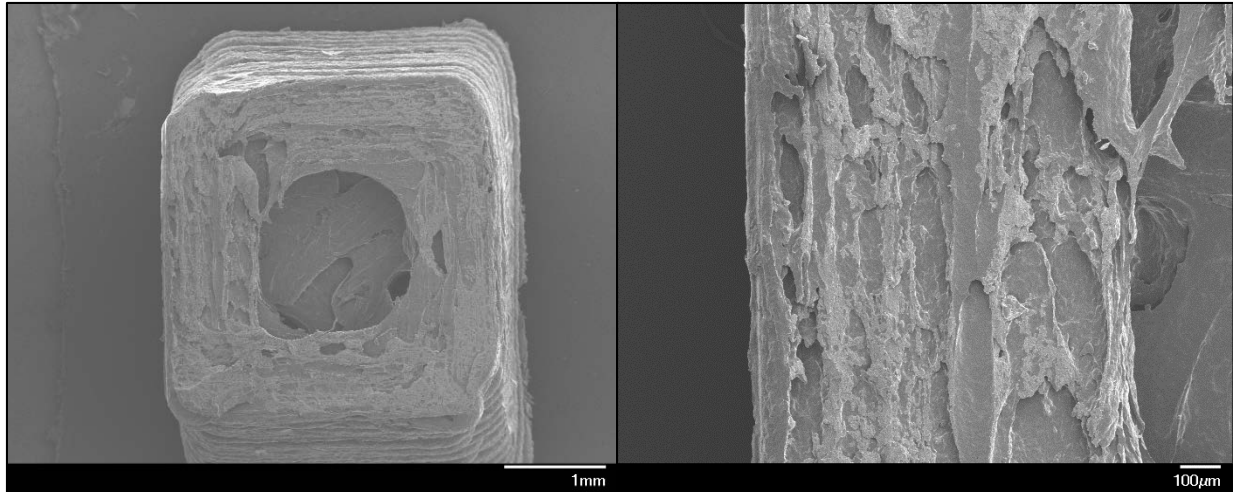


Figure 29: Micrograph of the U1222D showing poor inter-layer welding.

Figure 30 shows the full cross-section of the U2111E tensile bar. The perimeter was laid in a similar counterclockwise fashion as described for the 12222 prints: however, the 21112 print conditions had almost no protrusions caused by the perimeter pattern. Figure 30 shows that the 12222 prints had far better layer to layer welding and minimal gaps between the outer and inner perimeters. Figure 30 shows white areas where layer to layer welding occurred; however, there are many gaps between these welded areas. The gaps observed inside the layer may be caused by shear forces associated with the direction of flow as the print nozzle deposits layers. The extrusion temperature of 255°C is well above the  $T_g$  of the Ultimaker filament and may have caused the filament to flow non-homogeneously; thus leading to the ‘shear gaps’.





*Figure 30: (Left) Micrograph of the U2111E, showing rectangular perimeter, (Right) Micrograph of the perimeter-infill interface of the U2111E sample, showing non-homogeneous flow at layers.*

#### *4.4.3 Zortrax*

The two print condition IDs observed in this section are 12113 and 21123. The perimeters laid for all Zortrax prints were the most rectangular and had few artifacts or protrusions in the gage length of the tensile bars. Figure 31 shows the full cross-section of the Z1211B tensile bar. Figure 31 shows that the 12113 prints had minimal layer to layer welding and large gaps between the outer perimeter and infill raster. The whiter areas of the cross-section show where the layer to layer welding was formed.

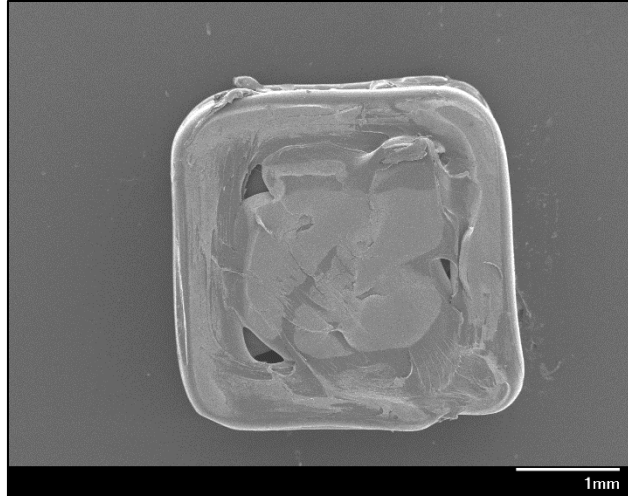


*Figure 31: Micrograph of the Z1211B sample, showing poor infill.*

Figure 32 shows the full cross-section of the Z2112B tensile bar. Figure 32 show that the 21123 prints had better layer to layer welding and minimal gaps between the outer perimeter and infill raster. The better inter-layer welding can be attributed to the high extrusion temperature and low layer thickness of the 21123 print condition. The Zortrax prints experienced no yielding during testing and no ductile fracture mechanisms.

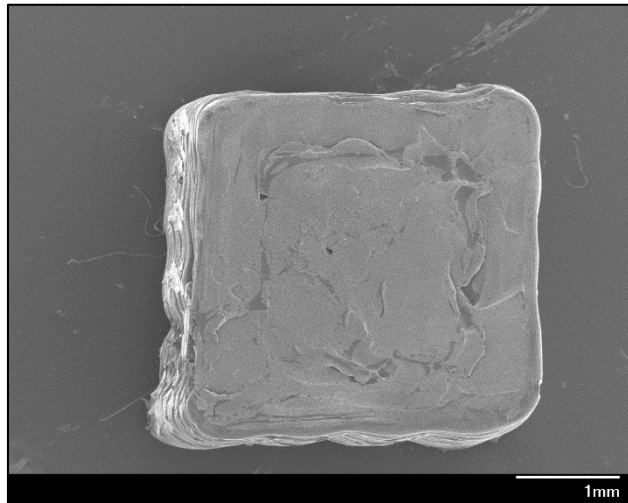


*Figure 32: Micrograph of the Z2112B sample, showing better infill.*

### 4.5 Principal Component Analysis

All the tensile strengths and elastic moduli were normalized for this section to account for the different cross-sectional areas produced by each of the three printers. The master data spreadsheet was then imported into the SAS JMP 14 statistical analysis software. Principal component analysis was run on the large dataset. Normalized tensile strength, elastic modulus, elongation to break, extrusion temperature, layer thickness, print bed temperature, and print speed were set as numerical variables. The print condition IDs, sample IDs, and printer type were set as characteristic values. Observed in the spree plots of Figure 33, PC1 and PC2 were determined to have the largest effect on the correlated eigenvalues for the numerical variables analyzed for each printer set (Figure 33). The MakerBot printer set had PC1 and PC2 with values of 45.282% and 32.768% respectively. The Ultimaker printer set had PC1 and PC2 with values of 60.080% and 32.736% respectively. The Zortrax printer set had PC1 and PC2 with values of 50.220% and 35.530% respectively.

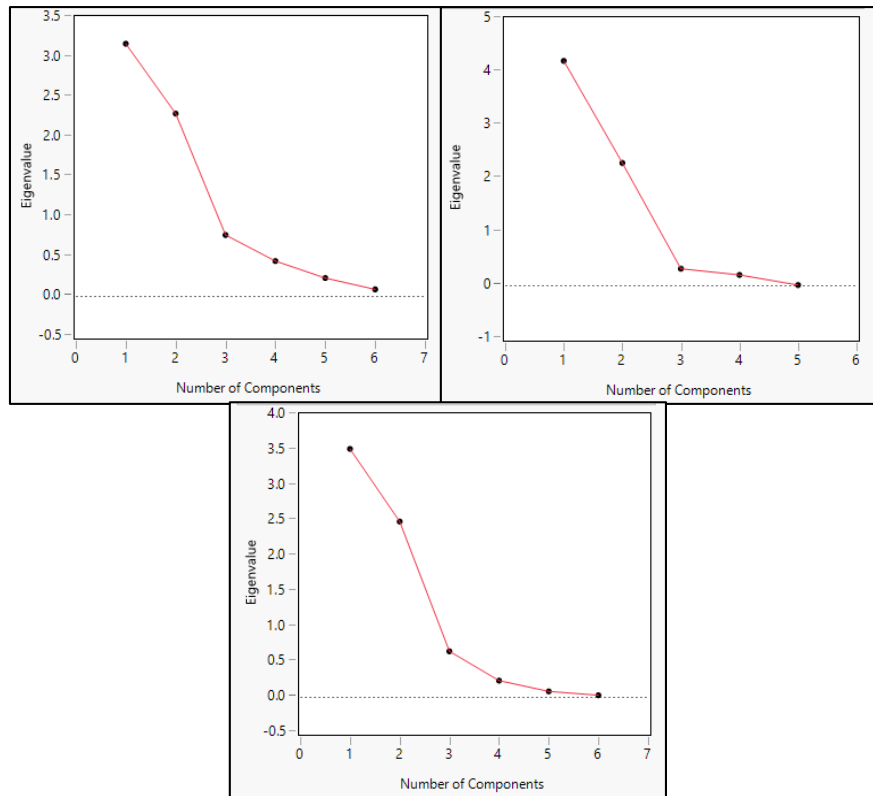


Figure 33: (Top left) Magnitude of effect of PCs on eigenvalues of MakerBot values, (Top right) Magnitude of effect of PCs on eigenvalues of Ultimaker values, (Bottom center) Magnitude of effect of PCs on eigenvalues of Zortrax values.

Figure 34, Figure 35, and Figure 36 graph the magnitude and direction of the eigenvalues in relation to PC1 and PC2 for each printer set. These graphs express which print conditions are correlated to each other and at which magnitude they are so. It was clear that printer selection had a massive effect on the print condition correlations. For each printer set, print conditions had different correlations to each other.

Figure 34 shows the eigenvalues from the MakerBot prints in relation to PC1 and PC2. The extrusion temperature (ET) is shown to have a strong correlation to the resulting normalized tensile strength (NTS) and elongation at break (EaB). For MakerBot prints, print speed (PS) is negative correlated with the resultant NTS. Print bed temperature (PBT) is shown to be positively correlated with the resulting normalized elastic modulus (NEM). This correlation likely does not indicate any relationship between these two parameters, for it has been shown through finite element analysis that PBT only has an effect on the first couple of layers in a print [8]. Moreover, layer thickness (LT) is shown to have a strong negative correlation to the resultant NEM. Table 2 shows which print conditions had a positive, negative, or negligible correlation to the investigated mechanical properties.

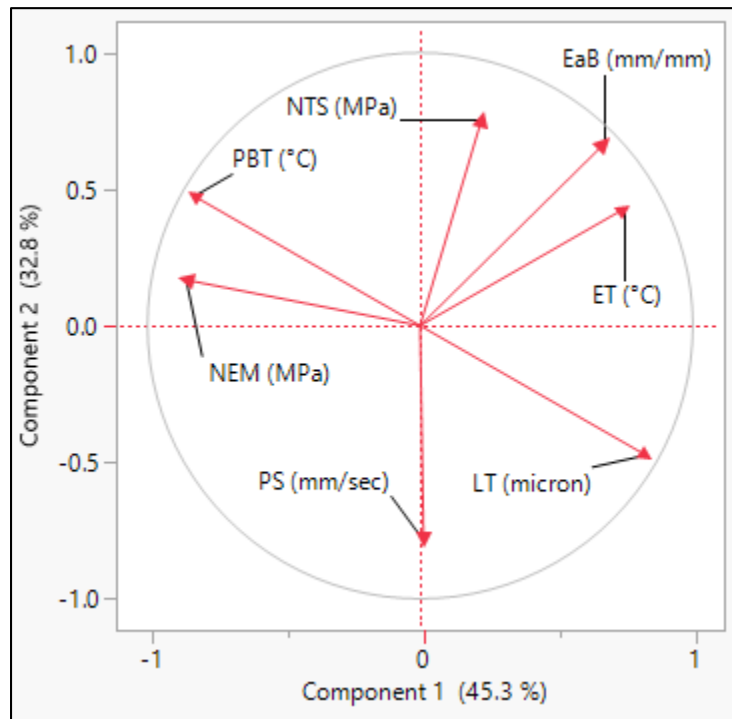


Figure 34: Eigenvalues from the MakerBot prints in relation to PC1 and PC2.

Table 2: Positive and negative correlations seen from PCA for MakerBot prints.

MakerBot Replicator 2X				
	ET	LT	PBT	PS
NTS	Positive	N/A	N/A	Negative
EaB	Positive	N/A	N/A	N/A
NEM	N/A	Negative	Positive	N/A

Figure 35 shows the eigenvalues from the Ultimaker prints in relation to PC1 and PC2. The ET is shown to have a positive correlation to the resulting NTS and a stronger positive correlation to EaB as found through tensile testing. PBT, PS, and LT are shown to have a negative correlation, all of similar magnitude, to NEM. Further, PBT, PS, and LT are shown to have minimal correlation to the NTS and EaB of the Ultimaker prints. Table 3 shows which print conditions had a positive, negative, or negligible correlation to the investigated mechanical properties.

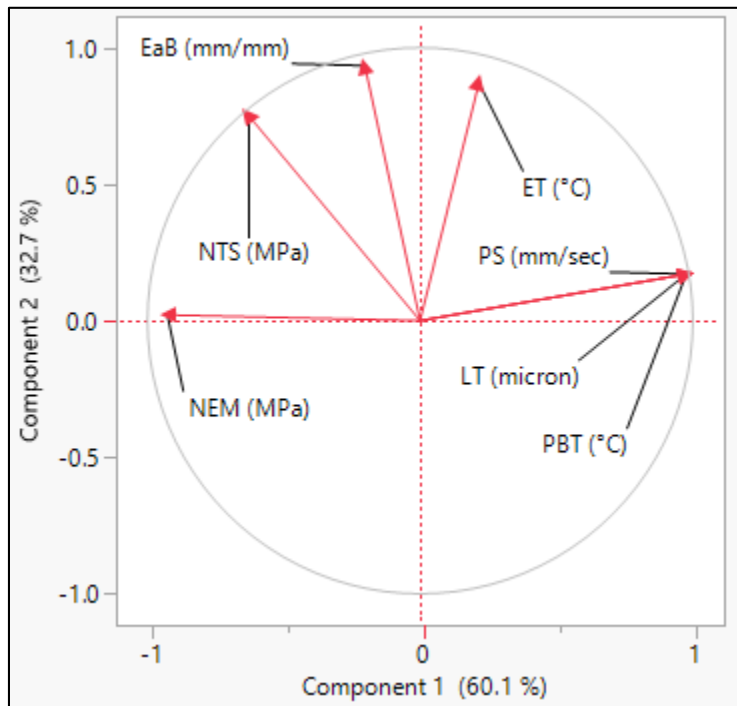


Figure 35: Eigenvalues from the Ultimaker prints in relation to PC1 and PC2.

Table 3: Positive and negative correlations seen from PCA for Ultimaker prints.

Ultimaker 3				
	ET	LT	PBT	PS
NTS	Positive	N/A	N/A	N/A
EaB	Positive	N/A	N/A	N/A
NEM	N/A	Negative	Negative	Negative

Figure 36 shows the eigenvalues from the Zortrax prints in relation to PC1 and PC2. ET is shown to have a strong positive correlation to the resulting NTS and EaB as found through tensile testing. PBT is shown to have a negligible correlation to the resulting mechanical properties of Zortrax prints. PS is shown to have a positive correlation to the resultant NEM. Further, LT is shown to have a strong negative correlation to the NEM of Zortrax prints. Table 4 shows which print conditions had a positive, negative, or negligible correlation to the investigated mechanical properties.

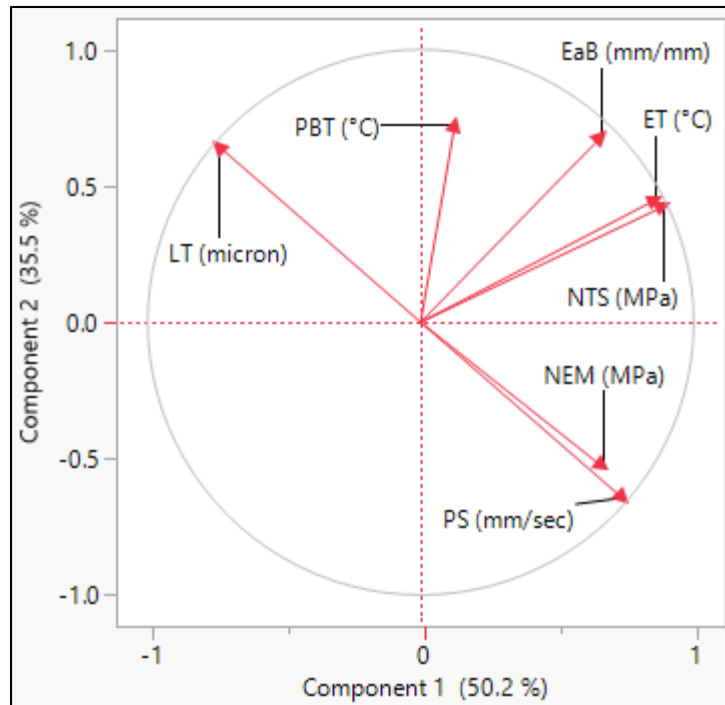


Figure 36: Eigenvalues from the Zortrax prints in relation to PC1 and PC2.

Table 4: Positive and negative correlations seen from PCA for Zortrax prints.

Zortrax M200				
	ET	LT	PBT	PS
NTS	Positive	N/A	N/A	N/A
EaB	Positive	N/A	N/A	N/A
NEM	N/A	Negative	N/A	Positive

## Summary & Conclusions

The two aims of this thesis were to 1) Use an informatics approach to design a workflow that would ensure the collection of high pedigree data from each stage of the printing process; 2) Apply the workflow, in conjunction with a DOE, to investigate FFF processing parameters.

ABS filament was used to print ASTM D638 Type V tensile bars. MakerBot Replicator 2X, Ultimaker 3, and Zortrax M200 were used to fabricate the tensile bars. Data was analyzed using PCA. DSC and DMA were used to characterize the filaments used. SEM was used to understand the mechanical fracture behaviors experienced during tensile testing.

It was found that extrusion temperature, layer thickness, print speed, and printer type were the printing conditions that had the greatest effect on resulting mechanical properties. Print bed temperature had little to no effect on the mechanical properties of all print conditions. Each printer saw a decrease in tensile strength and elongation at break when samples were printed at lower extrusion temperatures (210°C compared to 255°C). Elastic modulus was affected by both layer thickness and print speed. A smaller layer thickness (140µm compared to 290µm) had a positive effect on elastic moduli for all printers. The effect of print speed on the elastic modulus was more printer specific. Through PCA it was determined that printer selection drastically changed the magnitude of effect each print condition had on the resulting mechanical properties of each print.



## **Looking Forward**

Further investigation is needed to determine the sources of the differences in mechanical properties seen through this thesis. It is clear that the FFF community contains diverse materials and printers, each producing different outcomes from similar print conditions. By following an informatics workflow process, the relationship between good mechanical properties and high print quality should be investigated. From the data collected in this thesis, it can be hypothesized that mechanical properties and print quality may be inversely related. However, until there is more standardization between the materials and printers of the FFF and MEAM community, it may remain unclear as to the exact relationship between resultant print properties and selected print conditions.

## References

- [1] M. Nikzad, S. H. Masood and I. Sbarski, "Thermo-mechanical properties of a highly filled," Swinburne University of Technology, 2011.
- [2] M. Bogers, R. Hadar and A. Bilberg, "Additive manufacturing for consumer-centric business models: Implications for supply chains in consumer goods manufacturing," *Technological Forecasting and Social Change*, no. 102, pp. 225-239, 2016.
- [3] E. D. Bain, "Polymer Powder Feedstock Evaluation & Development of Selective Laser Sintering (SLS)," U.S. Army Research Laboratory , Aberdeen Proving Ground, MD, 2017.
- [4] T. Coogan and D. Kazmer, "Bond and part strength in fused deposition modeling," *Rapid Prototyping Journal*, vol. 23, no. 2, pp. 414-422, 2017.
- [5] C. Davis, K. Hillgartner, S. Han and J. Seppala, "Mechanical strength of welding zones produced by polymer extrusion additive manufacturing," *Additive Manufacturing*, no. 16, pp. 162-166, 2017.
- [6] K. Christiyan, U. Chandrasekhar and K. Venkateswarlu, "A study on the influence of process parameters on the Mechanical Properties of 3D printed ABS composite," *IOP Conference Series: Materials Science and Engineering*, no. 114, p. 12109, 2016.
- [7] H. Li, T. Wang, J. Sun and Z. Yu, "The effect of process parameters in fused deposition modelling on bonding degree and mechanical properties," *Rapid Prototyping Journal*, vol. 24, no. 1, pp. 80-92, 2018.
- [8] A. A. D'Amico, A. Debaie and A. M. Peterson, "Effect of layer thickness on irreversible thermal expansion and interlayer strength in fused deposition modeling," *Rapid Prototyping Journal*, vol. 23, no. 5, pp. 942-953, 2017.
- [9] M. Spoerk, J. Gonzalez-Gutierrez, J. Sapkota, S. Schuschigg and C. Holzer, "Effect of the printing bed temperature on the adhesion of parts produced by fused filament fabrication," *Plastics, Rubber and Composites*, vol. 47, no. 1, pp. 17-24, 2017.
- [10] K. Rajan, "Materials informatics," *Materials Today*, vol. 8, no. 10, pp. 38-45, 2005.

- [11] S. Kumar and J. P. Kruth, "Composites by rapid prototyping technology," Elsevier Ltd, 2009.
- [12] "Investigation of Polymers with Differential Scanning Calorimetry," Humboldt University of Berlin, 2015.
- [13] P. De, N. Choudhury, N. Dutta, A. Bhowmick and K. Shelat, "Thermal Analysis of Rubbers," ISmithers Rapra Pub., Shrewsbury, 2010.
- [14] Zortrax, Zortrax, 2018. [Online]. Available: <https://zortrax.com/>. [Accessed April 2018].
- [15] Ultimaker, Ultimaker B.V., 2018. [Online]. Available: <https://ultimaker.com/>. [Accessed April 2018].
- [16] MakerBot Industries, MakerBot Industries, 2018. [Online]. Available: <https://www.makerbot.com/>. [Accessed April 2018].
- [17] H. Hotelling, "Analysis of a complex of statistical variables into principal components," *The Journal of Educational Psychology*, no. 24, pp. 417-441 and 498-520, 1933.
- [18] S. Wold, K. Esbensen and P. Geladi, "Principal component analysis," *Chemometrics and Intelligent Laboratory Systems*, no. 2, pp. 37-52, 1987.
- [19] S. Bouhouche, L. L. Yazid, H. Tarek and B. Jurgen, "Inferential sensor – Based adaptive principal components analysis for mechanical properties prediction and evaluation," *Measurement*, no. 46, pp. 3683-3690, 2013.
- [20] D. Baccar and D. Soffker, "Identification and classification of failure modes in laminated composites by using a multivariate statistical analysis of wavelet coefficients," *Mechanical Systems and Signal Processing*, no. 96, pp. 77-87, 2017.
- [21] J. F. MacGregor and T. Kourti, "Statistical process-control of multivariate processes," *Control Engineering Practice*, no. 3, pp. 403-414, 1995.
- [22] M. A. Ryder, D. A. Lados, G. S. Iannacchione and A. M. Peterson, "Fabrication and properties of novel polymer-metal composites using fused deposition modeling," *Composites Science and Technology*, vol. 158, pp. 43-50, 2018.
- [23] J. M. G. Cowie, *Chemistry and Physics of Modern Materials*, 2nd Edition, CRC Press, 1991.

# Appendix A

## A.1 Print Set Form Example

Sample Set Form		
Operator Name:	Daniel Braconnier	
Date of Print:	1/23/2018	
CAD File Info		
Software:	SolidWorks2017	
File Type:	STL	
Print Material Info		
Material:	ABS	
Manufacturer:	MakerBot	
Lot ID:	003991	
Listed Additives:	N/A	
Lab Conditions		
Ambient Temp.:	21C	
Humidity:	26%	
Lab Usage:	Low	
Slicing Program		
Select Program:	Simplify3D	
Slicing Program Parameters		
Select Pattern:	22121	
Extrusion Temp.:	255C	
Layer Thickness:	290um	
Print Bed Temp.:	80C	
Print Speed:	35mm/s	
Print Orientation:	Vertical	
Raster Angles:	45/-45	
Printer Type		
Select Printer:	MakerBot Replicator 2X	
Sample IDs		
M	2212	A
M	2212	B
M	2212	C
M	2212	D
M	2212	E
M	2212	F
Projected Print Time		
N/A		
Actual Print Time		
N/A		
Quality of Print*		
3		
*On scales of 1 - 5		
Ease of Sample Removal*		
3		
Notes:		

Figure 37: Print set form filled out for the 22121 print condition.

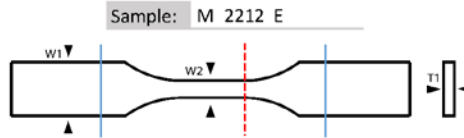
## A.2 Mechanical Test Form Example

Mechanical Test Form									
Operator Name: Daniel Braconnier									
Date of Print: 2/21/2018									
<b>ASTM Info</b>									
Test Type: D638									
Sample Type: V									
<b>Test Machine Info</b>									
Machine Type: Instron 5567A									
Model Number: 5567AR1986									
Last Calibration: 2/21/2018									
Load Cells: 65088									
<b>Sample IDs</b>									
M 2212 A									
M 2212 B									
M 2212 C									
M 2212 D									
M 2212 E									
M 2212 F									
<b>Lab Conditions</b>									
Ambient Temp.: 21C									
Humidity: N/A									
Lab Usage: Low									
<i>Take photos of each sample before and after they are tested and attach in PDF</i>									
<table border="1" style="width: 100%; border-collapse: collapse;"> <tr><td>Thickness (T1):</td><td>3.66mm</td></tr> <tr><td>Width1 (W1):</td><td>9.78mm</td></tr> <tr><td>Width2 (W2):</td><td>3.22mm</td></tr> <tr><td colspan="2" style="text-align: center;"><i>*Mark grip contacts and fracture point on diagram</i></td></tr> </table>	Thickness (T1):	3.66mm	Width1 (W1):	9.78mm	Width2 (W2):	3.22mm	<i>*Mark grip contacts and fracture point on diagram</i>		<p>Sample: M 2212 A</p>
Thickness (T1):	3.66mm								
Width1 (W1):	9.78mm								
Width2 (W2):	3.22mm								
<i>*Mark grip contacts and fracture point on diagram</i>									
<table border="1" style="width: 100%; border-collapse: collapse;"> <tr><td>Thickness (T1):</td><td>3.55mm</td></tr> <tr><td>Width1 (W1):</td><td>9.55mm</td></tr> <tr><td>Width2 (W2):</td><td>3.14mm</td></tr> <tr><td colspan="2" style="text-align: center;"><i>*Mark grip contacts and fracture point on diagram</i></td></tr> </table>	Thickness (T1):	3.55mm	Width1 (W1):	9.55mm	Width2 (W2):	3.14mm	<i>*Mark grip contacts and fracture point on diagram</i>		<p>Sample: M 2212 B</p>
Thickness (T1):	3.55mm								
Width1 (W1):	9.55mm								
Width2 (W2):	3.14mm								
<i>*Mark grip contacts and fracture point on diagram</i>									
<table border="1" style="width: 100%; border-collapse: collapse;"> <tr><td>Thickness (T1):</td><td>3.50mm</td></tr> <tr><td>Width1 (W1):</td><td>9.72mm</td></tr> <tr><td>Width2 (W2):</td><td>3.07mm</td></tr> <tr><td colspan="2" style="text-align: center;"><i>*Mark grip contacts and fracture point on diagram</i></td></tr> </table>	Thickness (T1):	3.50mm	Width1 (W1):	9.72mm	Width2 (W2):	3.07mm	<i>*Mark grip contacts and fracture point on diagram</i>		<p>Sample: M 2212 C</p>
Thickness (T1):	3.50mm								
Width1 (W1):	9.72mm								
Width2 (W2):	3.07mm								
<i>*Mark grip contacts and fracture point on diagram</i>									
<table border="1" style="width: 100%; border-collapse: collapse;"> <tr><td>Thickness (T1):</td><td>3.49mm</td></tr> <tr><td>Width1 (W1):</td><td>9.50mm</td></tr> <tr><td>Width2 (W2):</td><td>3.14mm</td></tr> <tr><td colspan="2" style="text-align: center;"><i>*Mark grip contacts and fracture point on diagram</i></td></tr> </table>	Thickness (T1):	3.49mm	Width1 (W1):	9.50mm	Width2 (W2):	3.14mm	<i>*Mark grip contacts and fracture point on diagram</i>		<p>Sample: M 2212 D</p>
Thickness (T1):	3.49mm								
Width1 (W1):	9.50mm								
Width2 (W2):	3.14mm								
<i>*Mark grip contacts and fracture point on diagram</i>									

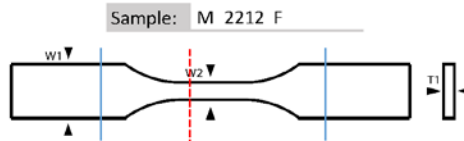
Figure 38: Mechanical test form filled out for the 22121 print condition (Page 1).

Mechanical Test Form

Thickness (T1):	3.48mm
Width1 (W1):	9.76mm
Width2 (W2):	3.13mm
*Mark grip contacts and fracture point on diagram	



Thickness (T1):	3.70mm
Width1 (W1):	9.63mm
Width2 (W2):	3.26mm
*Mark grip contacts and fracture point on diagram	



Notes:

All samples were hand placed without jig for the gage section was too large for jig.

2/21/2018

Page 2

Figure 39: Mechanical test form filled out for the 22121 print condition (Page 2).

## Appendix B

### *B.1 Micrographs of 12121 & 21211 Print Conditions*

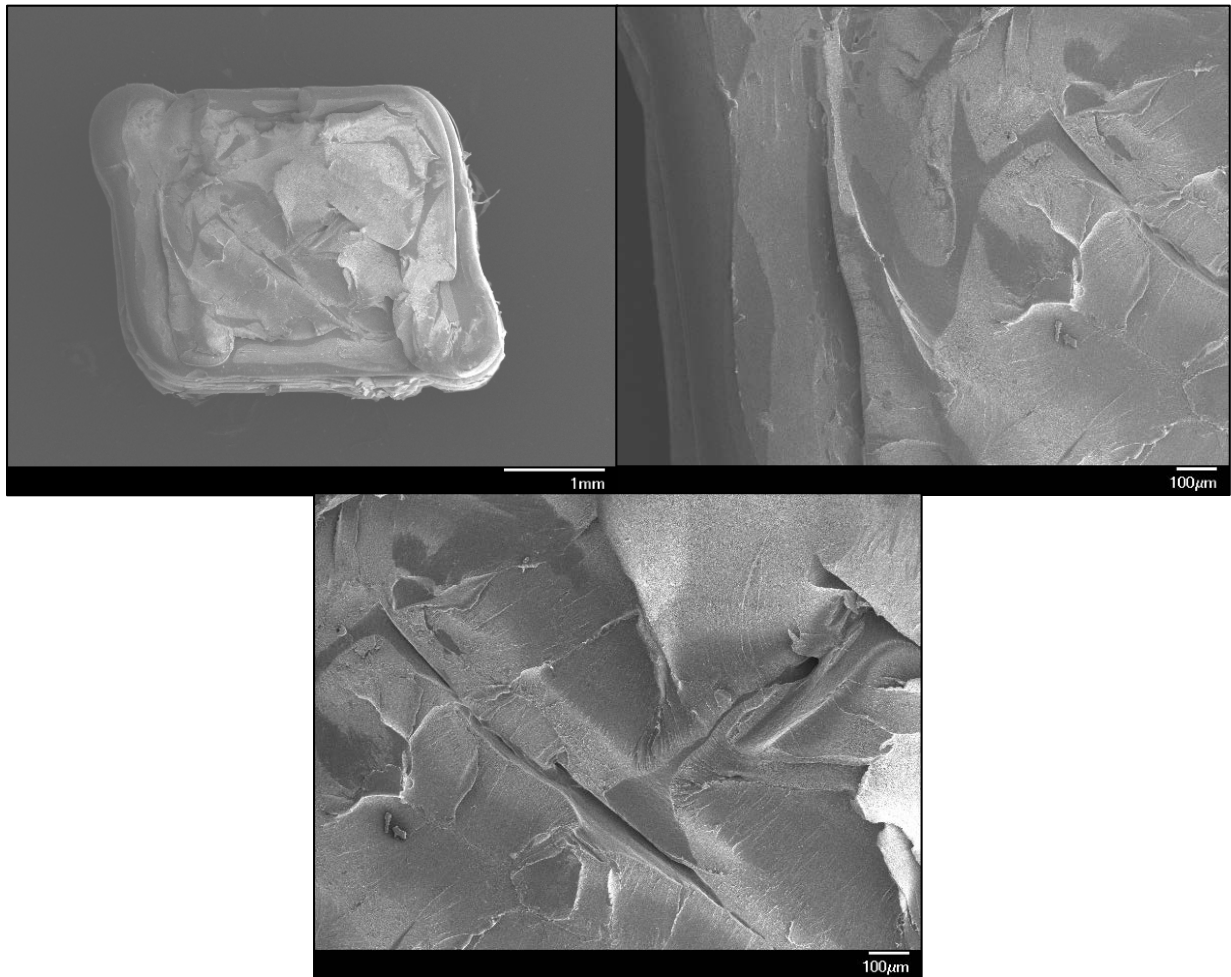


*Figure 40: (Top left) Full cross-section of M1212B sample, (Top right) Perimeter edge of M1212B sample, (Bottom center) Center of M1212B sample.*

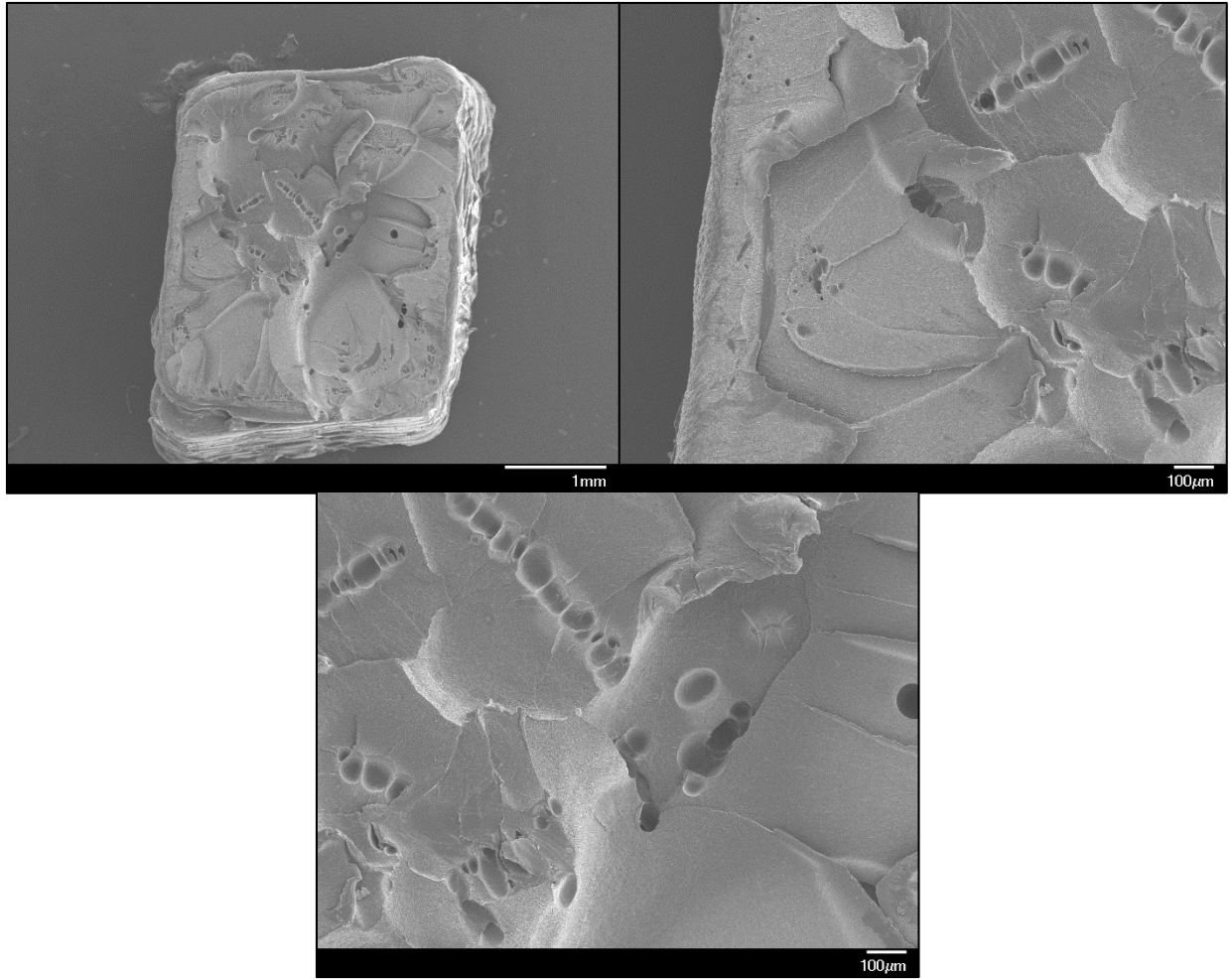


*Figure 41: (Top left) Full cross-section of M1212D sample, (Top right) Perimeter edge of M1212D sample, (Bottom center) Center of M1212D sample.*



*B.2 Micrographs of 12222 & 21112 Print Conditions*

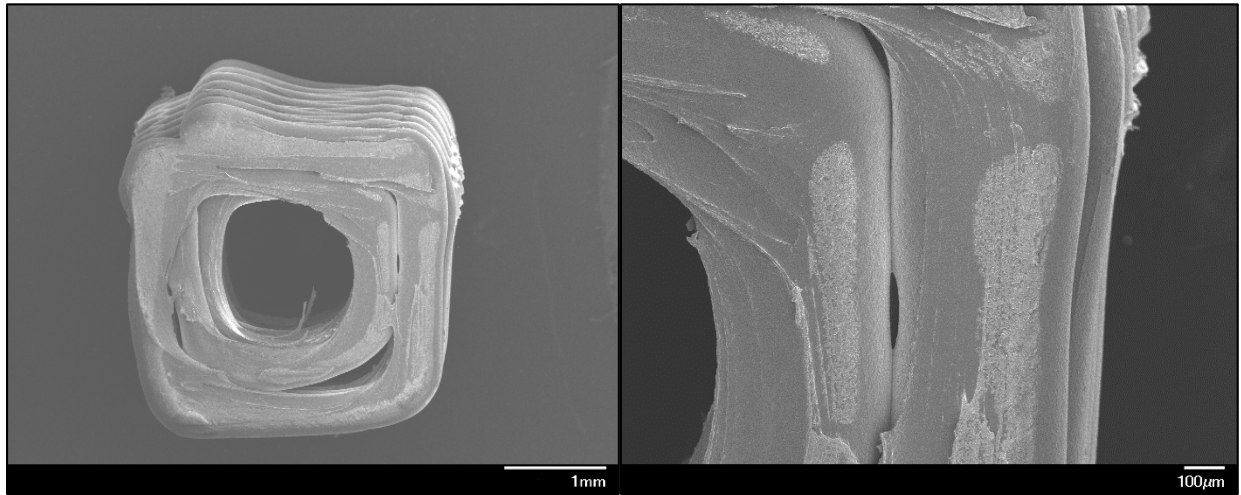


*Figure 42: (Top left) Full cross-section of U1222D sample, (Top right) Perimeter edge of U1222D sample, (Bottom center) Center of U1222D sample.*

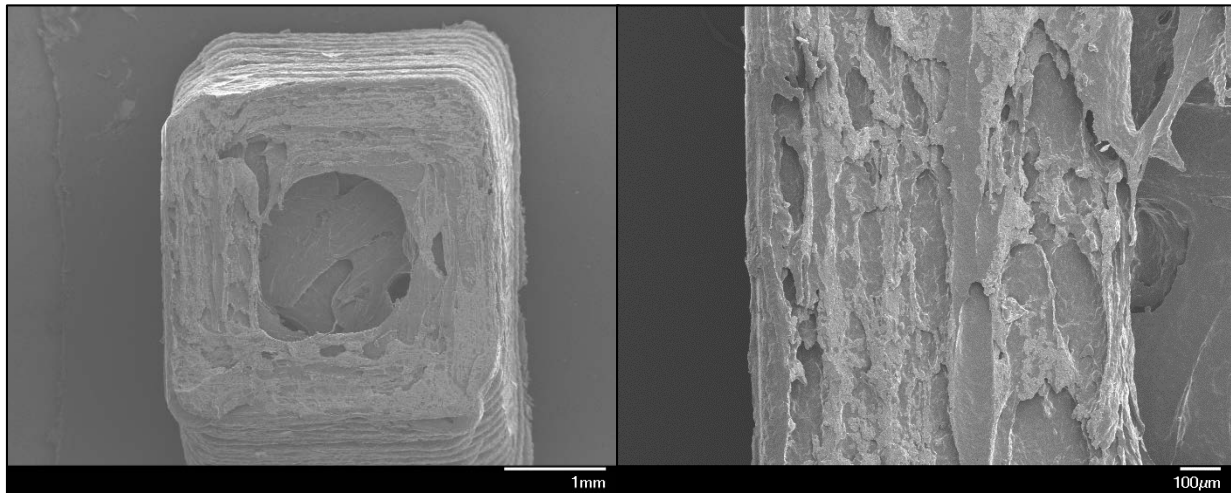


*Figure 43: (Top left) Full cross-section of U2111E sample, (Top right) Perimeter edge of U2111E sample, (Bottom center) Center of U2111E sample.*

*B.3 Micrographs of 12113 & 21123 Print Conditions*

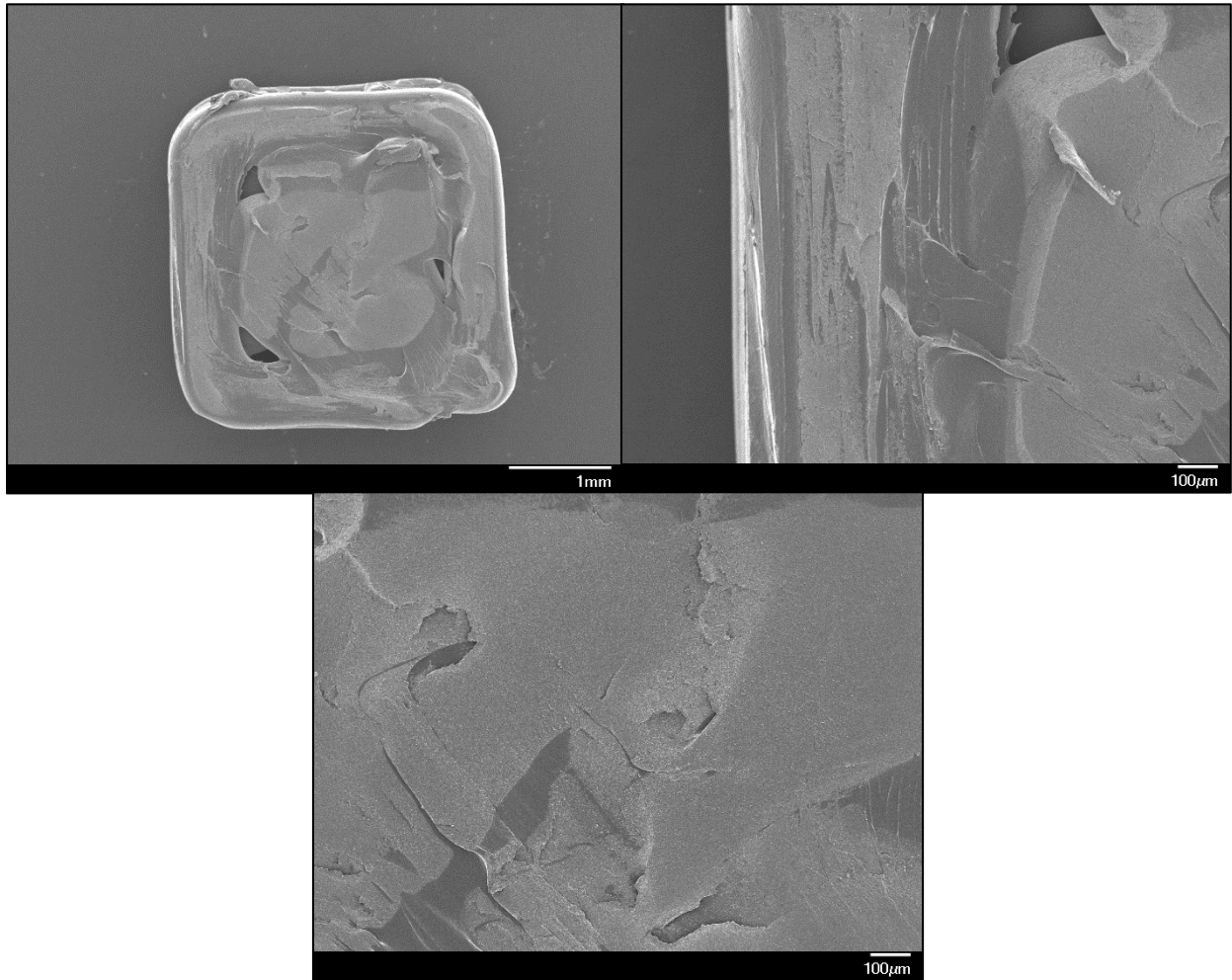


*Figure 44: (Top left) Full cross-section of Z1211B sample, (Top right) Perimeter edge of Z1211B sample, (Bottom center) Center of Z1211B sample.*

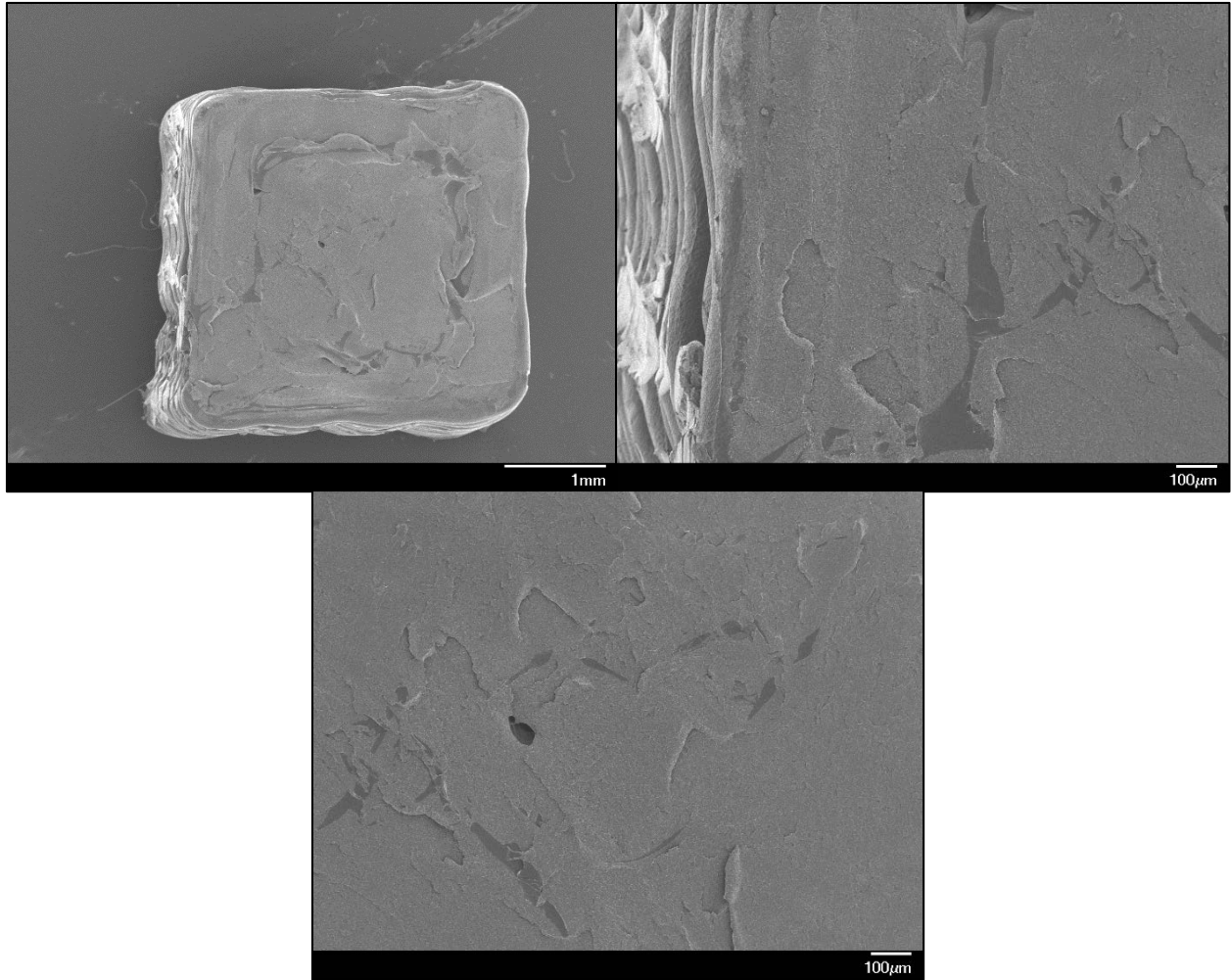


*Figure 45: (Top left) Full cross-section of Z2112B sample, (Top right) Perimeter edge of Z2112B sample, (Bottom center) Center of Z2112B sample.*